

RESEARCH ARTICLE

Dissection of Nidogen function in *Drosophila* reveals tissue-specific mechanisms of basement membrane assembly

Jianli Dai¹, Beatriz Estrada², Sofie Jacobs^{1,2a}, Besaiz J. Sánchez-Sánchez^{2,2b}, Jia Tang^{1,2c}, Mengqi Ma¹, Patricia Magadán-Corpas², José C. Pastor-Pareja^{1,3*}, María D. Martín-Bermudo^{2*}

1 School of Life Sciences, Tsinghua University, Beijing, China, **2** CABD (CSIC-Universidad Pablo de Olavide-JA), Seville, Spain, **3** Peking-Tsinghua Center for Life Sciences, Beijing, China

^{2a} Current address: Rega Institute, KU Leuven, Leuven, Belgium

^{2b} Current address: Randall Centre for Cell and Molecular Biophysics, King's College London, London, United Kingdom

^{2c} Current address: School of Forestry and Biotechnology, Zhejiang Agriculture and Forestry University, Hangzhou, China

* jose.pastor@biomed.tsinghua.edu.cn (JCP-P); mdmarber@upo.es (MDM-B)



OPEN ACCESS

Citation: Dai J, Estrada B, Jacobs S, Sánchez-Sánchez BJ, Tang J, Ma M, et al. (2018) Dissection of Nidogen function in *Drosophila* reveals tissue-specific mechanisms of basement membrane assembly. *PLoS Genet* 14(9): e1007483. <https://doi.org/10.1371/journal.pgen.1007483>

Editor: Claude Desplan, New York University, UNITED STATES

Received: June 11, 2018

Accepted: August 20, 2018

Published: September 27, 2018

Copyright: © 2018 Dai et al. This is an open access article distributed under the terms of the [Creative Commons Attribution License](https://creativecommons.org/licenses/by/4.0/), which permits unrestricted use, distribution, and reproduction in any medium, provided the original author and source are credited.

Data Availability Statement: All relevant data are within the paper and its Supporting Information files.

Funding: This work was supported by the Ministerio Español de Ciencia y Tecnología (grant number BFU2016-80797 to MDM-B) and by the NSFC (grants number 31771600 and 31371459 to JCP-P). BJS-S was supported by a FPI studentship from the MCYT. The institutional support from the Junta de Andalucía to the CABD is acknowledged. The funders had no role in study, design, data

Abstract

Basement membranes (BMs) are thin sheet-like specialized extracellular matrices found at the basal surface of epithelia and endothelial tissues. They have been conserved across evolution and are required for proper tissue growth, organization, differentiation and maintenance. The major constituents of BMs are two independent networks of Laminin and Type IV Collagen in addition to the proteoglycan Perlecan and the glycoprotein Nidogen/entactin (Ndg). The ability of Ndg to bind in vitro Collagen IV and Laminin, both with key functions during embryogenesis, anticipated an essential role for Ndg in morphogenesis linking the Laminin and Collagen IV networks. This was supported by results from cultured embryonic tissue experiments. However, the fact that elimination of Ndg in *C. elegans* and mice did not affect survival strongly questioned this proposed linking role. Here, we have isolated mutations in the only Ndg gene present in *Drosophila*. We find that while, similar to *C. elegans* and mice, *Ndg* is not essential for overall organogenesis or viability, it is required for appropriate fertility. We also find, alike in mice, tissue-specific requirements of *Ndg* for proper assembly and maintenance of certain BMs, namely those of the adipose tissue and flight muscles. In addition, we have performed a thorough functional analysis of the different Ndg domains in vivo. Our results support an essential requirement of the G3 domain for Ndg function and unravel a new key role for the Rod domain in regulating Ndg incorporation into BMs. Furthermore, uncoupling of the Laminin and Collagen IV networks is clearly observed in the larval adipose tissue in the absence of Ndg, indeed supporting a linking role. In light of our findings, we propose that BM assembly and/or maintenance is tissue-specific, which could explain the diverse requirements of a ubiquitous conserved BM component like Nidogen.

collection and analysis, decision to publish, or preparation of the manuscript.

Competing interests: The authors have declared that no competing interests exist.

Author summary

Basement membranes (BMs) are thin layers of specialized extracellular matrices present in every tissue of the human body. Its main constituents are two networks of laminin and Type IV Collagen linked by Nidogen (Ndg) and proteoglycans. They form an organized scaffold that regulates organ morphogenesis and function. Mutations affecting BM components are associated with organ dysfunction and several congenital diseases. Thus, a better comprehension of BM assembly and maintenance will not only help to learn more about organogenesis but also to a better understanding and, hopefully, treatment of these diseases. Here, we have used the fruit fly *Drosophila* to analyse the role of Ndg in BM formation *in vivo*. Elimination of Ndg in worms and mice does not affect survival, strongly questioning its proposed linking role, derived from *in vitro* experiments. Here, we show that in the fly, Ndg is dispensable for BM assembly and preservation in many tissues, but absolutely required in others. Furthermore, our functional study of the different Ndg domains challenges the significance of some interactions between BM components derived from *in vitro* experiments, while confirming others, and reveals a new key requirement for the Rod domain in Ndg function and incorporation into BMs.

Introduction

Basement membranes (BM) are specialized thin extracellular matrices underlying all epithelia and endothelia, and surrounding many mesenchyme cells. This thin layer structure, which appears early in development, plays key roles in the morphogenesis, function, compartmentalization and maintenance of tissues [1].

All BMs contain at least one member of the Laminin, Type IV Collagen (Col IV), proteoglycan Agrin and Perlecan, and Nidogen (Entactin) families. Nidogen is a 150-kDa glycoprotein highly conserved in mammals, *Drosophila*, *Caenorhabditis elegans* (*C. elegans*) and ascidians [2, 3]. Nidogens have been proposed to play a key role in BM assembly by providing a link between the Laminin and Col IV networks and by integrating other ECM proteins, such as Perlecan, into this specialized extracellular matrix [4–7]. While invertebrates possess only one Nidogen, two Nidogen isoforms, Nid1 and Nid2, have been identified in vertebrates. The individual knock out of either *Nid1* or *Nid2* in mice does not affect BM formation or organ development [8–10]. In fact, these *Nid1* or *Nid2* null animals appear healthy, fertile and have a normal life span. However, simultaneous elimination of both isoforms results in perinatal lethality, with defects in the lung, heart and limb development that are not compatible with postnatal survival [11, 12]. In addition, BM defects are only observed in certain organs, which strongly suggests tissue-specific roles for Nidogens in BM assembly and function [11]. Like in mice, loss of the only Nidogen-encoding gene in *C. elegans*, *NID-1*, is viable with minor defects in egg laying, neuromuscular junctions and position of longitudinal nerves, but no defects in BM assembly [13–15]. Altogether, these studies reveal that Nidogen may play important roles in specific contexts, consistent with its evolutionary conservation. However, the different requirements for Nidogens in BM assembly and organogenesis in mice and *C. elegans* suggest that new functions may have arisen in vertebrates. The isolation of mutants in Nidogen in other organisms will help to shed light on the role of the Nidogen proteins *in vivo* and its conservation throughout evolution.

All Nidogens comprise three globular domains, namely G1, G2 and G3, one flexible linker connecting G1 and G2, and one rod-shaped segment, composed primarily of epidermal growth factor repeats, separating the G2 and G3 domains [4, 16, 17]. A number of studies using recombinant fragments of Nidogens have provided a wealth of information on the

structure and binding properties of the different Nidogen domains in vitro. Thus, key roles have been proposed for the globular domains G3 and G2 in mediating interactions of Nidogen with the Laminin network and with the Collagen IV network, respectively [4, 7, 17–20]. Despite this, the relevance of these interactions in vivo remains to be established. Furthermore, some of the predictions from cell culture and in vitro experiments do not hold when tested in model organisms. For example, deletion of the G2 domain in *C. elegans* is viable and does not affect organogenesis [14]. Furthermore, it has been shown that Ndg1 and Ndg2 do not form molecular cross-bridges between the Laminin and Collagen IV networks in the epidermal BM of human skin [21]. These results in animal models are inconsistent with a role for Nidogen as a generally essential linker between the Collagen IV and Laminin networks, leaving open the question of whether in vivo Nidogen functions at all as a linker.

Drosophila BMs are analogous to the vertebrate ones [22]. They cover the basal surface of all epithelia and surround most organs and tissues, including muscles and peripheral nerves. Even though their composition might vary according to tissues and developmental stages, all *Drosophila* BMs contain Col IV, Laminin, Perlecan and Nidogen. However, in contrast to the three Col IV, sixteen Laminins and two Nidogens found in humans, *Drosophila* only produces one Col IV, two distinct Laminins and one Nidogen (Ndg). The reduced number of ECM components, which limits the redundancy among them, and their high degree of conservation with their mammalian counterparts, makes *Drosophila* a perfect model system to dissect their function in vivo. *Drosophila* Col IV has been identified as a homolog of mammalian Type IV Collagen, which is a long helical heterotrimer that consists of two $\alpha 1$ chains and one $\alpha 2$ chain encoded by the genes *Collagen at 25 C* (*Cg25C*) and *viking* (*vkg*), respectively [23–25]. The C terminal globular non-collagenous (NC1) domain and the N terminal 7S domain interact to form the Col IV network [26]. Loss of function mutations in either of the two *Col IV* genes in flies affect muscle development, nerve cord condensation, germ band retraction and dorsal closure, causing embryonic lethality [27]. In addition, mutations in Col IV have been associated with immune system activation, intestinal dysfunction and shortened lifespan in the *Drosophila* adult [28]. Finally, while Col IV deposition in wing imaginal discs and embryonic ventral nerve cord (VNC) BMs is not required for localization of Laminins and Nidogens, it is essential for Perlecan incorporation [29, 30]. The *Drosophila* Laminin $\alpha\beta\gamma$ trimer family consists of two members comprised of two different α subunits encoded by *Laminin A* and *wing blister*, one β and one γ subunits encoded by *Laminin B1* and *Laminin B2*, respectively [31]. Same as Col IV, Laminin trimers can also self-assemble into a scaffold through interactions of the N-terminal LN domains located in their short arms [32]. Elimination of Laminins in *Drosophila* affects the normal morphogenesis of most organs and tissues, including the gut, muscles, tracheae and nervous system [33, 34]. In addition, abnormal accumulation of Col IV and Perlecan was observed in Laminin mutant tissues [33]. Perlecan, encoded by the *trol* (*terribly reduced optic lobes*) gene, is subdivided into five distinct domains. Interactions with Laminins and Col IV occur through domains I and V (reviewed in [35]). Mutations in *trol* affect postembryonic proliferation of the central nervous system, plasmatocytes and blood progenitors [36–38]. Loss of *trol* also affects the ultrastructure and deposition of Laminins and Col IV in the ECM around the lymph gland [38]. Altogether, these results suggest that BM components Laminin, Col IV and Perlecan are all essential for proper development. In addition, they also reveal a hierarchy for their incorporation into BMs that seems to be tissue-specific and required for proper BM assembly and function. In this context, however, the role of Ndg in *Drosophila* morphogenesis and BM assembly has remained elusive. This may be in part due to the lack of mutations in this gene.

In this work, we have dissected the role of Ndg in *Drosophila*. Using a newly generated anti-Ndg antibody, we have shown that Ndg accumulates in the BMs of embryonic, larval and adult

tissues. By isolating several mutations in the single *Drosophila Ndg* gene, we find that while, similar to *C. elegans* and mice, *Ndg* is not required for overall organogenesis or viability, it is required for fertility. Also similar to the tissue-specific defects in mice and *C. elegans*, we find that the BMs surrounding the larval fat body and flight muscles of the notum are disrupted in the absence of *Ndg*. Furthermore, we observed uncoupling of laminin and Collagen IV in the fat body of *Ndg* mutants, indeed supporting a role of *Ndg* as a linker between the two networks. In addition, we have performed a thorough functional analysis of the different *Ndg* domains in vivo, which, on one hand, supports an essential requirement of the G3 domain for *Ndg* function and, on the other hand, uncovers a new key role for the Rod domain in regulating *Ndg* incorporation into BMs. Finally, we find that BM assembly is not universal but differs depending on the tissue and propose that this could explain the diverse requirements of a ubiquitous conserved BM component like Nidogen.

Results

Nidogen localizes to the BM of embryonic, larval and adult tissues

Previous analysis has shown that, during embryogenesis, *Ndg* is expressed in multiple mesodermal cell types, such as visceral mesoderm, somatic muscle founder cells, a subset of pericardial and cardial cells and at the edges of the visceral mesoderm [39–41]. Here, we decided to further analyse *Ndg* expression in embryonic, larval and adult tissues. In order to do this, an antibody against a peptide encoded by exon 7 was developed (see [Materials and Methods](#)). We found that in addition to the pattern described previously, similar to Laminins [33], *Ndg* was also detected in the BM surrounding most embryonic tissues in stage 16 embryos, including muscles, ventral nerve cord (VNC) and gut ([Fig 1A, 1A', 1B and 1B'](#)). However, in contrast to Laminins, *Ndg* was not enriched at muscle attachment sites ([Fig 1A](#)). In addition, a careful analysis of *Ndg* expression in stage 13 embryos revealed a dotted pattern along the visceral mesoderm, which differs from the continuous line observed around the muscles or the VNC ([Fig 1C and 1C'](#)). At this stage, caudal visceral mesodermal cells migrate over the visceral mesoderm. In fact, using a marker for these cells, *croc-lacZ* [42], we found that *Ndg* accumulated around them as they migrate ([Fig 1C and 1C'](#)). In this case, *Ndg* seems to be organized in track-like arrays, similar to the distribution of laminins around migrating hemocytes. *Ndg* was also found in migrating hemocytes, as visualized using a version of Nidogen tagged with superfolder GFP (sGFP), expressed from a duplication of the *Ndg* genomic region ([Fig 1D, \[43\]](#)). Finally, *Ndg* was also found at high levels in chordotonal organs ([Fig 1A and 1A'](#), asterisk). These results suggest that as it is the case for Laminins, *Ndg* can be deposited and/or assembled in different patterns throughout embryogenesis.

In addition, and similar to the other BM components, *Ndg* was found in the BMs that surround most larval tissues, including fat body, imaginal discs, tracheae, salivary glands, midgut, mature muscles and heart ([Fig 1E and Fig 2](#)), as well as in the follicular epithelium of the adult ovary ([Fig 1F](#)).

Fat body adipocytes and blood cells are the main source of Nidogen in larval BMs

A recent study has shown that macrophages are the major producers of BM components in the *Drosophila* embryo [30]. To investigate the cellular origin of Nidogen in the developing fly, we designed a GAL4-driven, UAS-controlled short hairpin against sGFP to eliminate sGFP-tagged Nidogen without disrupting normal function of endogenous untagged Nidogen ([Fig 2A](#)). This approach (isGFPi, for *in vivo* sGFP interference) is similar to iGFPi (*in vivo* GFP

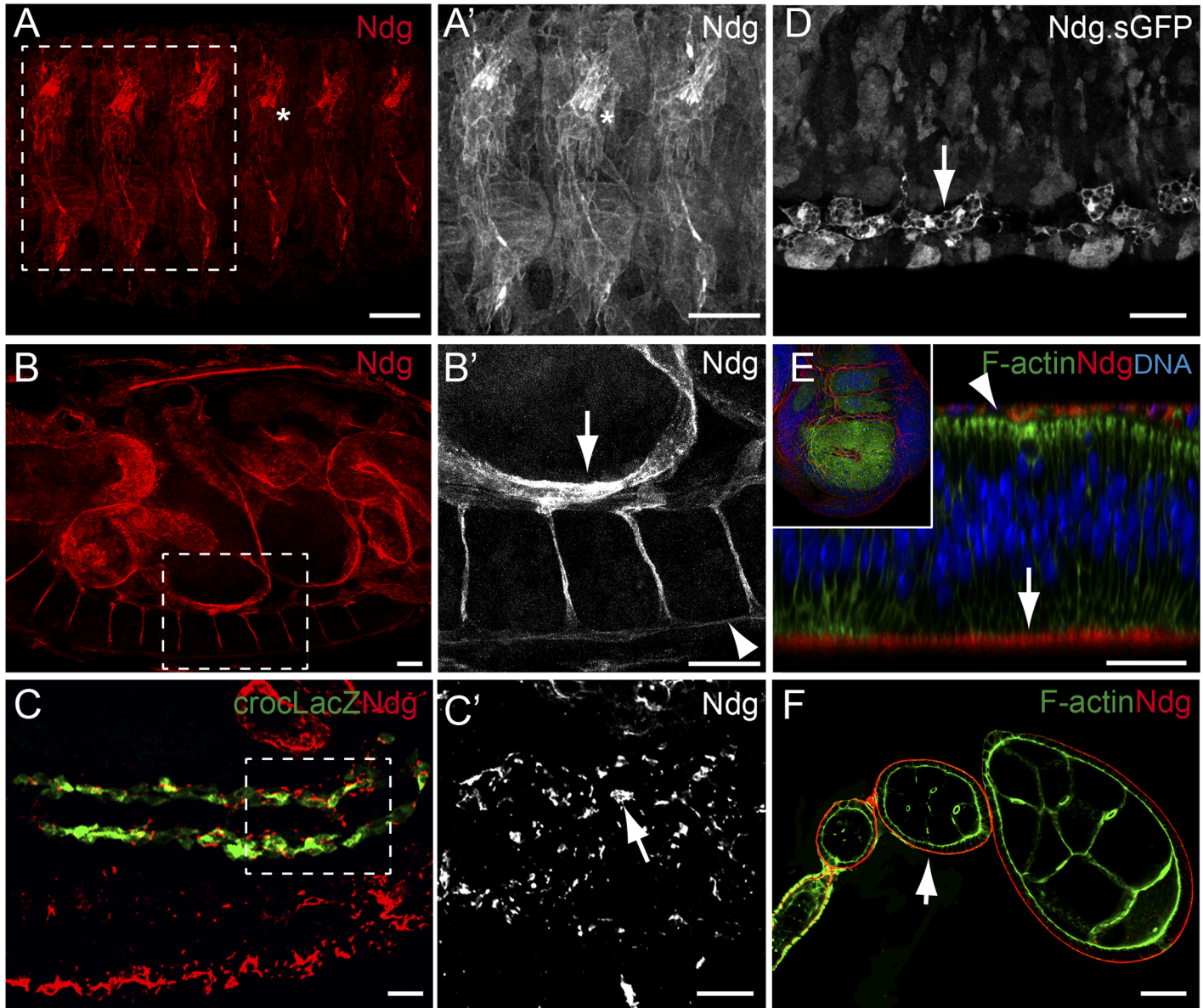


Fig 1. Distribution of the Ndg protein. (A-F) Confocal images showing embryonic (A-D), wing imaginal disc (E), and ovarian tissues (F) stained with anti-Ndg (A-C, and E-F) or anti-GFP (NdgsGFP, D). (A, B) In stage 16 wild-type embryos, Ndg (red) is found in the BMs surrounding most tissues, including muscles (A, A'), gut (B, B' (arrow) and VNC (B, B', arrowhead) and in chordotonal organs (asterisk). (C, C') Lateral view of a stage 13 embryo showing Ndg (red) accumulation around caudal visceral mesodermal cells visualized with the marker *crocLacZ* (green, arrow in C'). (D) Ndg is found in embryonic macrophages (arrow). (E) Ndg (red) is found at the basal surface of wing imaginal disc epithelial cells (arrow) and cells of the peripodial membrane (arrowhead). (F) Ndg (red) accumulates in the basement membrane (BM) around the follicular epithelium (arrow). Scale bars represent 20µm (A-F).

<https://doi.org/10.1371/journal.pgen.1007483.g001>

interference, [29, 44] and iYFPi [45], which we previously used to show that fat body adipocytes are the major source of Collagen IV and Perlecan in the larva. We found here that isGFPi knock down of Ndg.sGFP driven by Cg-GAL4, which drives expression in fat body and blood cells (*Cg>isGFPi*), reduced the presence of Ndg.sGFP in the whole animal. Ndg.sGFP signal was largely reduced or undetectable in most tissues, including fat body itself, imaginal discs, tracheae, midgut and heart (Fig 2B). Deposition of Ndg.sGFP was only partially reduced in the VNC, the imaginal ring of the salivary gland and body wall muscles, and was not visibly affected in myoblasts (Fig 2B), suggesting that some larval tissues besides the fat body could

Fig 2. Fat body adipocytes and blood cells are the main source of Ndg in larval BMs. (A) Schematic representation of the in vivo sGFP interference approach (isGFPi). (B) Confocal images showing the localization of functional Ndg.sGFP fusion protein expressed under control of the endogenous promoter in different tissues of the 3rd instar larva. Images compare tissues from control larvae (+) and larvae where Ndg.sGFP expression has been knocked down in fat body adipose tissue and blood cells (*Cg>isGFPi*). Ndg.sGFP signal is not observed in the BMs of *Cg>isGFPi* larvae, except in wing disc myoblasts (asterisk) and partially in the imaginal ring of the salivary gland, body wall muscles and VNC (purple arrows). Note that Ndg.sGFP signal disappears from myoblasts when isGFPi is driven with myoblast driver *Mef2-GAL4* (*Mef2>isGFPi*). Arrow and circles in the fat body panel indicate BM and CIVICs (Collagen IV Intercellular Concentrations), respectively. In tracheal images, apical cuticle autofluorescence is observed in the tracheal lumen (downward-pointing yellow arrow). Nuclei stained with DAPI (white).

<https://doi.org/10.1371/journal.pgen.1007483.g002>

produce their own Ndg. To test this in the case of myoblasts, we induced isGFPi with muscle-specific *Mef2-GAL4* [46], and found that Ndg.sGFP disappeared from notum myoblasts (*Mef2>isGFPi*, Fig 2B), proving that they produce their own Nidogen. These results show that, as it is the case for Collagen IV, fat body and blood cells are the main source of Ndg in the larva, but also that exceptions to this rule exist.

We next decided to assess the origin of the three other core BM components by performing the same assay for sGFP-tagged Laminin B1, GFP-tagged Col IV and YFP-tagged Perlecan (S1A Fig). We found that, similar to Nidogen, fat body and blood cells are the main source of the BM components of all tissues, except myoblasts and partially the VNC (S1A Fig). Component-specific exceptions were tracheal cells with regard to Perlecan, the imaginal rings of the salivary glands for Perlecan and Laminin, and finally imaginal discs for Laminin (S1A Fig). Indeed, *LanB1* knock down in the wing disc under control of *en-GAL4* reduced presence of Laminin in the corresponding region of the disc, proving the ability of imaginal discs to secrete part or all of their Laminin (S1B Fig). In all, our results show that although the four core BM components are largely produced by fat body adipocytes and blood cells during larval stages, other tissues may also be able to provide them. Consistently, Ndg mRNAs have been detected in muscle founder cells [39], while Laminin mRNAs [47] and Laminin protein secretion [48] have been shown in the developing VNC.

Generation of Nidogen mutant alleles

The *Drosophila* genome contains a single *Ndg* gene. To analyse *Ndg* requirements during development, we isolated a series of deficiencies uncovering the gene *Ndg* (Fig 3A, S2 Fig; see Materials and Methods). These deficiencies were all homozygous lethal. However, as they removed other genes (S2 Fig), we could not draw conclusions from this result. Therefore, we next took advantage of the CRISPR-Cas9 technology to isolate a series of specific *Ndg* alleles that would allow us to study *Ndg* function (Fig 3A; see Materials and methods). To generate *Ndg* null alleles, embryos were injected with Cas9 mRNA and a combination of four sgRNAs designed against the 5'UTR exon (sgRNA1), exon 3 (sgRNA2 and sgRNA3) and exon 8 (sgRNA4). Two mutant lines in which the intervening *Ndg* sequence between sgRNA1 and sgRNA4 had been deleted partially (*Ndg*¹) or completely (*Ndg*²) were isolated (Fig 3A). Gene CG3422, contained between exons 9 and 10 of the *Ndg* gene was not perturbed. Both mutations are predicted to be *Ndg* null alleles because of absence of a transcription start site. In fact, qRT-PCR, using different primers along the *Ndg* gene (Fig 3A), showed no mRNA expression in *Ndg*¹ homozygous mutant larvae compared to wild type controls (Fig 3B). Furthermore, consistent with *Ndg*¹ and *Ndg*² being null alleles, staining with our Ndg antibody could not detect presence of the protein in larval or embryonic tissues (Fig 3C and 3D, S3D Fig).

As domain G3 has been postulated to be critical for binding of Ndg to Laminins, we also isolated *Ndg* mutant alleles in which this domain and the adjacent Rod domain were eliminated (Δ Rod-G3 alleles) in order to analyze its function in the context of the whole organism.

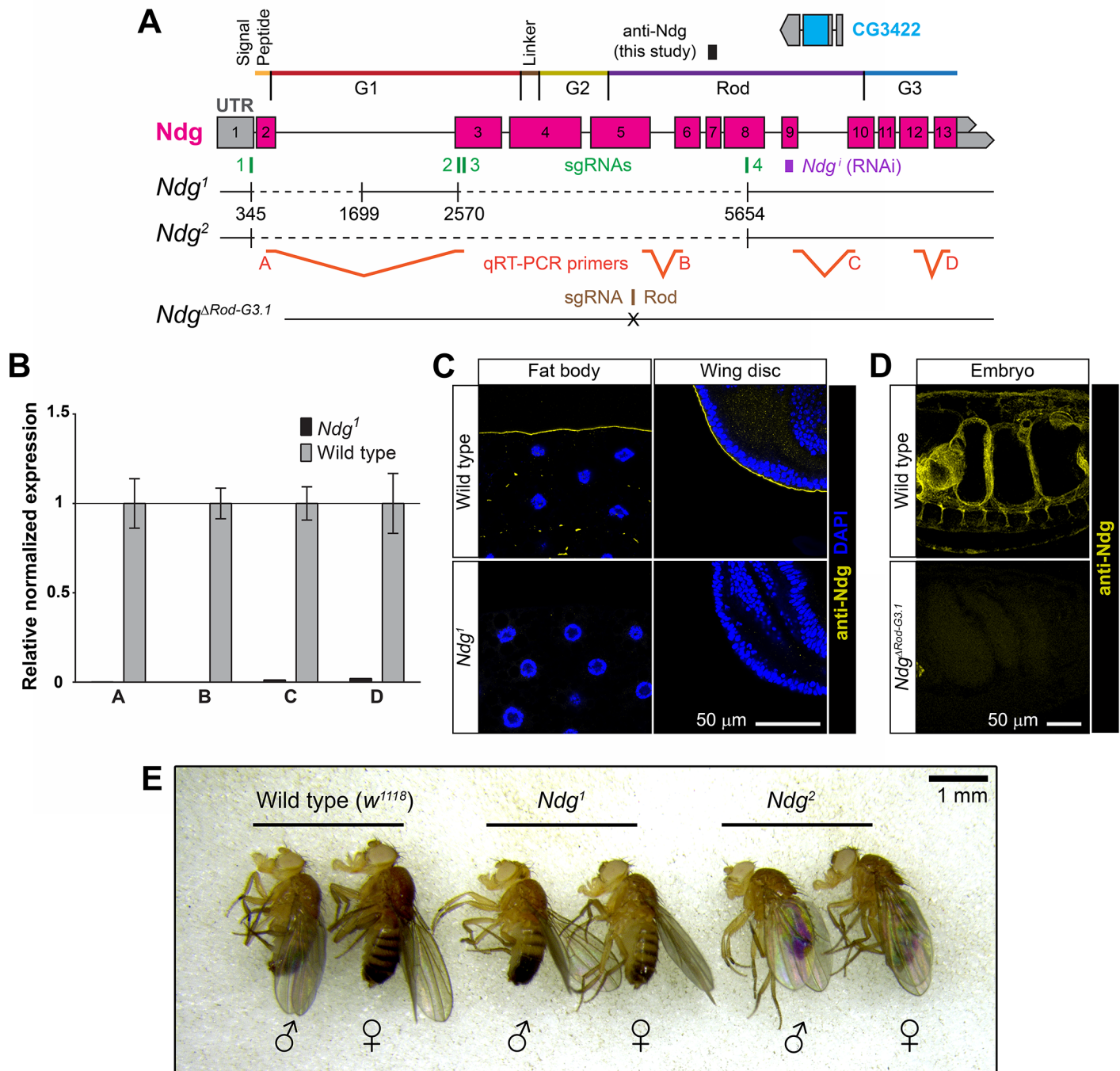


Fig 3. CRISPR/Cas9-generated Nidogen mutants are viable. (A) Schematic representation of the *Ndg* locus (2nd chromosome), *Ndg* mutants generated, sgRNAs used for generation of mutants (green boxes, 1–4), sequence targeted by *Ndg* RNAi construct (purple box, *Ndg*¹), epitope recognized by the rabbit anti-*Ndg* antibody generated in this study (black box) and qRT-PCR primers used to molecularly characterize the *Ndg*¹ mutant (A–D). (B) Expression of *Ndg* mRNA in wild type (*w*¹¹¹⁸) and *Ndg*¹ homozygous mutant larvae, assessed by qRT-PCR. Error bars represent 95% confidence intervals from three repeats. (C, D) Confocal images of larval fat body (C, left panels), wing imaginal discs (C, right panels) and embryos (D) from wild type (upper panels), *Ndg*¹ (C, lower panels) and *Ndg*^{ΔRod-G3.1} (D, lower panel) mutant animals stained with anti-*Ndg* antibody (yellow). (C) Nuclei stained with DAPI (blue). (E) Homozygous *Ndg*¹ and *Ndg*² mutants are viable and show no obvious morphological abnormalities.

<https://doi.org/10.1371/journal.pgen.1007483.g003>

In this case, transgenic lines stably expressing an sgRNAs against exon 5 were generated and crossed to flies expressing Cas9 (see [Materials and Methods](#)). Three mutant alleles, $Ndg^{ARod-G3.1}$, $Ndg^{ARod-G3.2}$ and $Ndg^{ARod-G3.3}$, were selected ([Fig 3A](#)). Two of them, $Ndg^{ARod-G3.1}$, $Ndg^{ARod-G3.2}$, were deletions of five and eight base pairs that resulted in frame-shifts generating stop codons eight and seven amino acids after the shift, respectively. In the other one, $Ndg^{ARod-G3.3}$, six base pairs were replaced by seven different ones, generating a frame-shift and a stop codon right after the shift. As expected, no staining using the antibody generated in this study was detected in $Ndg^{ARod-G3.1}$ homozygous embryos ([Fig 3D](#) and [S3 Fig](#)).

All CRISPR/Cas9 *Ndg* mutant alleles we generated were homozygous viable with no obvious morphological abnormalities ([Fig 3E](#)). These data show that, in contrast to double *Nid1 Nid2* knock out mice and similar to *C. elegans Nid-1* mutants, *Ndg* is dispensable for viability in *Drosophila*. In addition, similar to *C. elegans* [14], elimination of *Ndg* results in reduced fertility in flies ([S4A Fig](#)). However, in contrast to the phenotype observed when removing Laminins, Col IV or Perlecan [22, 49], no defects were observed in the shape of eggs laid by *Ndg* mutant females ([S4B Fig](#)).

Nidogen is required for integrity of the BM of the larval fat body and adult flight muscles

Once shown that *Ndg* mutant flies are viable, we decided to analyze the effects of *Ndg* loss in the BMs of the fly. We could not detect defects in most of the BMs we analyzed, including those present in the embryo, larval epidermis, imaginal discs, salivary glands, gut, muscles, VNC and the follicular epithelium in the ovary. However, we did observe a clear defect in the BM surrounding the larval fat body ([Fig 4A](#)). The larval fat body is an organ formed by large polyploid cells (adipocytes) covered by a BM that separates it from the hemolymph [50]. This BM contains, besides *Ndg*, the other three major components of BMs: Col IV, Laminins and Perlecan. Using tagged versions of these proteins, we found that the BM surrounding the fat body adipose tissue of Ndg^1 mutant larvae showed many holes, in contrast to the continuous appearance of the BM in wild type controls ([Fig 4A](#)). This phenotype was also observed when we knocked down *Ndg* expression using Cg-GAL4 (Ndg^1 , [Fig 4A](#)) and in the fat body of transheterozygous Ndg^1/Ndg^2 and $Ndg^1/Df(2R)BSC281$ larvae ([Fig 4B](#)). Furthermore, loss of BM integrity was additionally displayed by transheterozygous $Ndg^1/Ndg^{ARod-G3.1}$ fat body ([Fig 4B](#)), indicating a strong requirement of the Rod and G3 domains for this *Ndg* function. Confirming that this phenotype reflected a loss of *Ndg* function, the *Ndg*.sGFP transgene (see [Fig 2B](#)) rescued the integrity of fat body BMs in Ndg^1 mutants ([Fig 4C](#)).

We next investigated whether adipose tissue physiology was affected in *Ndg* mutants. Similar to human adipose, a major role of insect fat body is storage of neutral lipids. We stained fat body adipocytes with neutral lipid dye BODIPY and found that the lipid content in Ndg^1 and Ndg^2 mutant adipocytes was reduced, with some cells clearly presenting fewer and smaller lipid droplets than controls ([Fig 4D and 4E](#)). Quantification of lipid droplet diameter confirmed a significant reduction in droplet size in *Ndg* mutant larvae ([Fig 4E](#)). This result indicates a mild effect of *Ndg* loss in the physiology of these cells, suggesting inefficient lipid adsorption or intracellular metabolism.

In addition to fat body BM defects observed in Ndg^1 mutant larvae, we further discovered BM integrity defects in the flight muscles of the notum in *Ndg* mutant flies ([S4C Fig](#)). In addition, while flies appeared to fly normally and negative geotaxis climbing assays did not show differences with the wild type (not shown), Chill Coma Recovery Time (CCRT) assays [51] showed increased recovery times after cold exposure in flies lacking *Ndg*, suggesting mild behavioral or motor defects ([S4D Fig](#)).

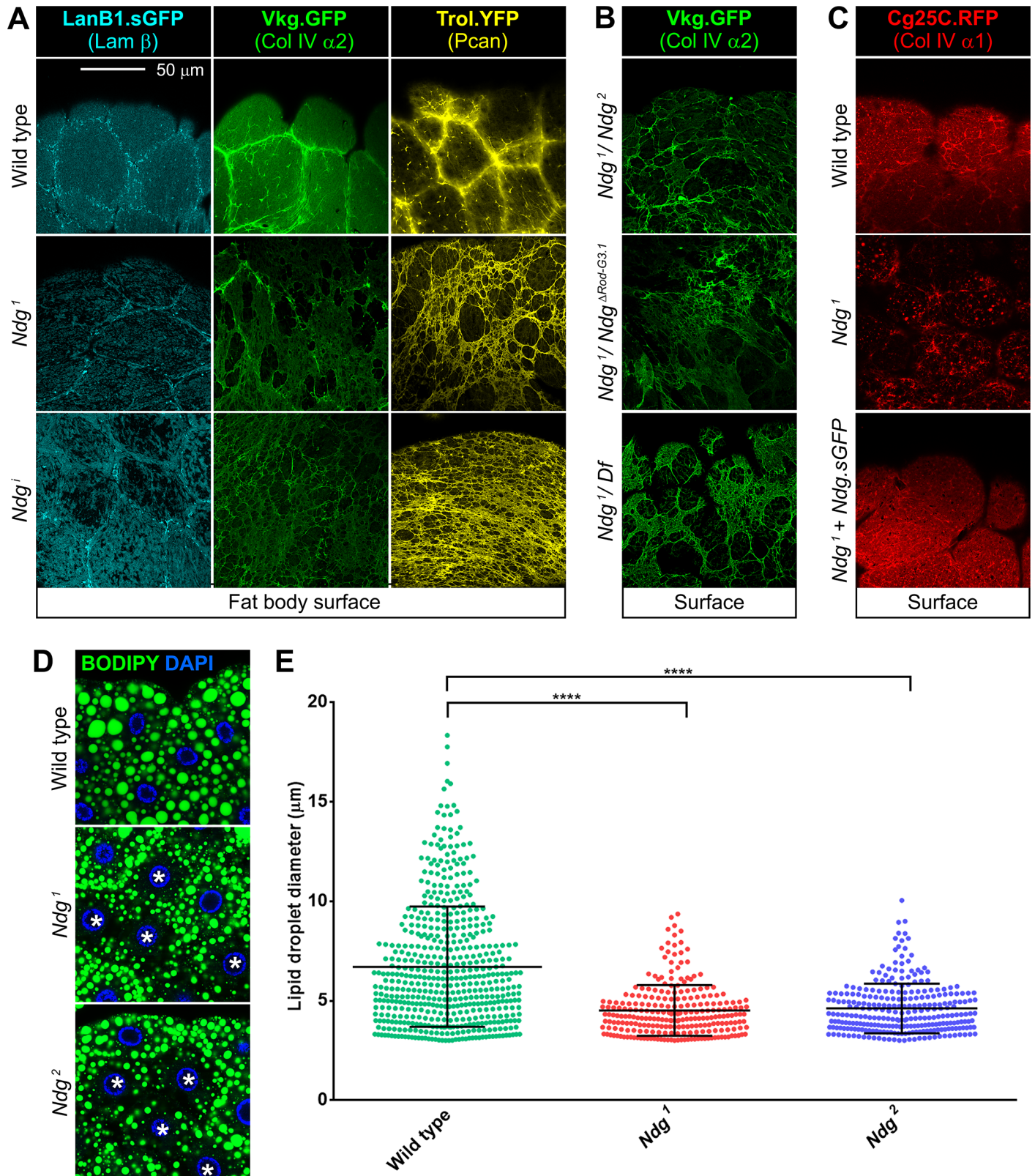


Fig 4. *Ndg* mutants show discontinuous adipose tissue BMs. (A) Confocal images of the larvae fat body BM showing localization of Laminin (LanB1.sGFP, cyan), Collagen IV (Vkg.GFP, green) and Perlecan (Trol.YFP, yellow) from control (upper panels), *Ndg¹* mutant (middle panels) and larvae where *Ndg* has been knocked

down under control of Cg-GAL4 (*Ndgⁱ*, lower panels). Loss of *Ndg* causes discontinuity of adipose tissue BMs. (B) Discontinuous BMs (Vkg.GFP, green) in the larval fat body of transheterozygotes *Ndg¹/Ndg²* (upper panel), *Ndg¹/Ndg^{ARod-G3.1}* (middle panel) and *Ndg¹/Ndg^{Df(2R)BSC281}* (lower panel). (C) Fat body BM (Cg25C.RFP, red) in wild type, *Ndg¹* mutant and *Ndg¹* mutant rescued with *Ndg.sGFP*. (D) Lipid droplets (neutral lipid dye BODIPY, green) in fat body of wild type (upper panel), *Ndg¹* mutant (middle panel) and *Ndg²* mutant (lower panel) larvae. Asterisks point to cells with reduced content of lipid droplets. Nuclei stained with DAPI (blue). Scale bar represents 50µm (A-D). (E) Quantification of lipid droplet diameter in 16 cells from wild type control, *Ndg¹* and *Ndg²* mutants. Each dot represents a single droplet. Particles smaller than 3µm in diameter were excluded from the analysis. Horizontal lines indicate the mean value and error bars represent ±SD. Difference with the wild type are significant in non-parametric Mann-Whitney tests (****: $p < 0.0001$).

<https://doi.org/10.1371/journal.pgen.1007483.g004>

In summary, our results show that although *Ndg* is not critically essential for fly development and assembly of most BMs, it is necessary for the integrity of BMs around specific tissues, such as the larval fat body and the adult flight muscles, and for appropriate fertility and fitness of the fly.

Functional analysis of the different Nidogen domains

In order to better understand the function of *Ndg*, we performed a functional analysis of the different *Ndg* domains. To do that, we generated transgenic flies capable of expressing GFP-tagged versions of the protein as well as mutant variants lacking one or several domains (Fig 5A) and tested their ability to localize to the BM of wing discs when expressed in fat body and blood cells. We carried out this localization analysis in the wing disc because *Ndg* present at wing disc BMs is produced by fat body and blood cells (Fig 2B) and because successful incorporation into the BM of a mutant GFP-tagged *Ndg* protein after secretion can be easily discerned in this tissue through confocal imaging. All the mutant variants we generated retain the signal peptide of full length *Ndg* to ensure correct secretion. Confirming secretion of all of them into the hemolymph, GFP signal was detected in the kidney-like pericardial cells (S5C Fig), known to filter the hemolymph and concentrate proteins present in it [52].

When expressed in the fat body and blood cells under control of the Cg-GAL4 driver, full length *Ndg* (*Ndg^{FL}.GFP*) was able to localize to the BMs of imaginal discs, as expected (Fig 5B). A similar analysis of the localization properties of the deletion constructs showed that no single domain of the protein was capable by itself to confer localization to BMs, suggesting cooperative interactions among domains are required for BM localization (Fig 5B). In addition, analysis of the localization of proteins in which a single domain was deleted (*Ndg^{ΔG1}*, *Ndg^{ΔG2}*, *Ndg^{ΔG3}* and *Ndg^{ΔRod}*) indicated that the only domain absolutely required for BM localization was the Rod domain, as *Ndg^{ΔRod}* was incapable of localizing to the BM of imaginal discs or other larval tissues (Fig 5B, S6 Fig). However, the Rod domain was insufficient to drive protein localization on its own (*Ndg^{Rod}*), but required the presence of the G2 or the G3 domains (*Ndg^{G2Rod}* and *Ndg^{RodG3}*, respectively; Fig 5B). This result is also supported by our analysis of the localization of *Ndg* in our *Ndg^{ARod-G3}* mutant embryos using an antibody raised against the G2 domain of *Ndg* [34] (S3 Fig). Staining with this antibody showed that the mutant protein *Ndg^{ARod-G3}*, lacking the Rod and G3 domains, did not localize to embryonic BMs, but it was still present in the chordotonal organs (S3B Fig). Altogether, our results show that the Rod domain is required but not sufficient for *Ndg* BM localization. They also show that G2+Rod and Rod+G3 are minimal alternative units capable of conferring BM localization to the *Ndg* protein, with G1 enhancing G2+Rod dependent-localization.

As mentioned in the introduction, analysis of the binding properties of *Ndg* domains and crystal structure have suggested that the G3 domain binds to Laminin, whereas the G2 domain binds to Col IV, with no clear function ascribed so far to the G1 domain. To investigate this in vivo, we assayed the localization abilities of the *Ndg^{ΔG1}*, *Ndg^{ΔG2}* and *Ndg^{ΔG3}* mutant proteins in the BMs of fat bodies where the expression of either Laminins or Col IV had been knocked down. We found that knock-down of *LanA* or *Cg25C*, encoding a Laminin α chain and Col IV

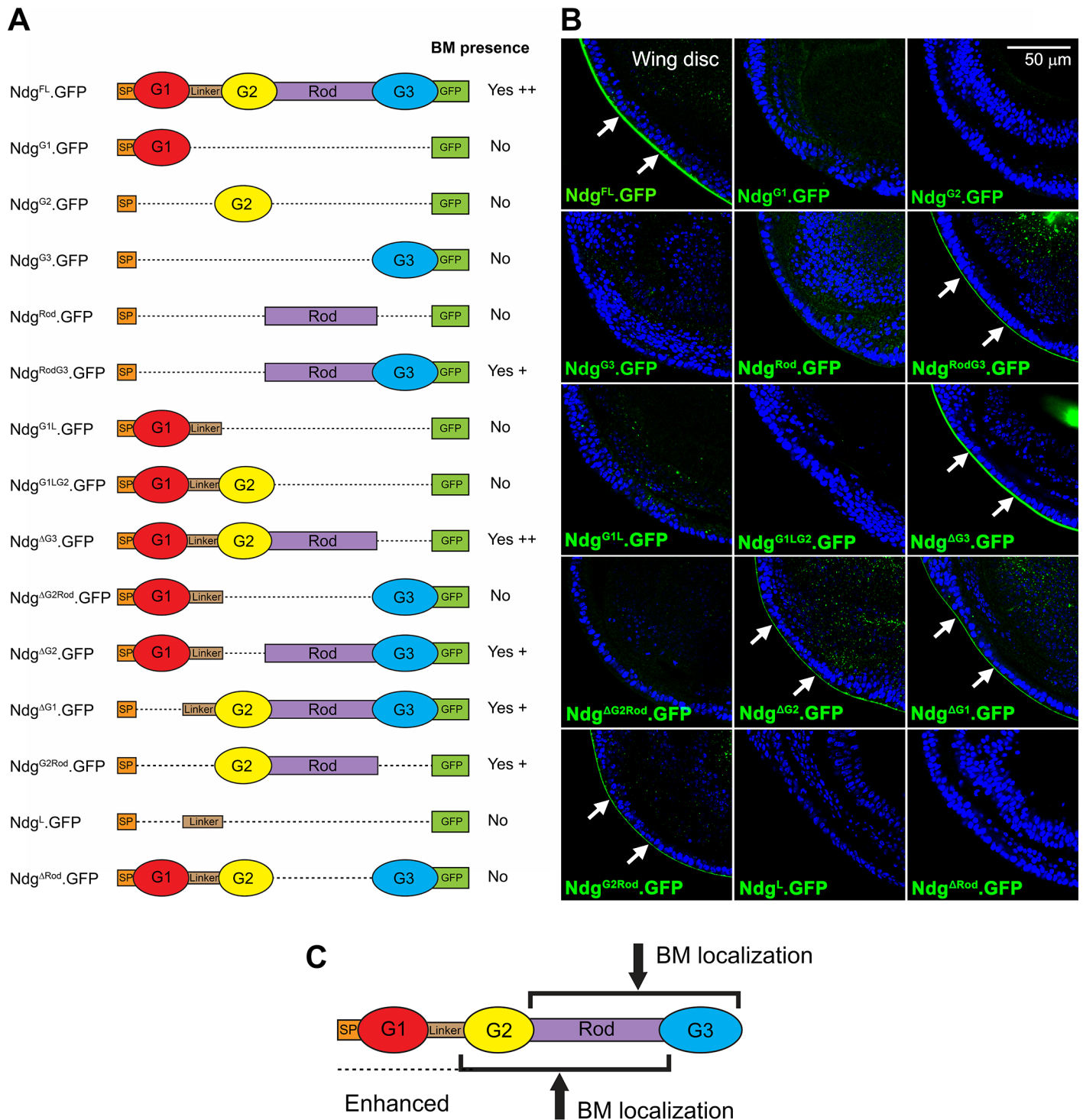


Fig 5. Rod domain is necessary but not sufficient for Nidogen localization to BMs. (A) Schematic depiction of Ndg full length (FL) and different Ndg deletions tested in this study. All Ndg versions are tagged with GFP in the C-terminal. SP = Signal Peptide. G1/2/3 = Globular domains 1/2/3. (B) Confocal images of wing discs from larvae expressing the indicated versions of Ndg under control of Cg-GAL4. Correct BM localization, detected by GFP signal (green, arrows), is observed only for Ndg versions containing the Rod domain (Ndg^{FL}, Ndg^{RodG3}, Ndg^{ΔG3}, Ndg^{ΔG2}, Ndg^{ΔG1} and Ndg^{G2Rod}) but neither Ndg^{Rod} nor any other single domain can localize to the BM by itself. Nuclei stained with DAPI (blue). (C) Model of domain requirements for proper Ndg localization to BMs.

<https://doi.org/10.1371/journal.pgen.1007483.g005>

$\alpha 1$, caused a marked reduction in the incorporation of full length Ndg^{FL}.GFP (Fig 6A–6C). In addition, while knocking down *LanA* had no effect on Ndg^{AG3} localization, *LanA* loss caused a marked reduction in the localization of both Ndg^{AG1} and Ndg^{AG2} (Fig 6A and 6B). Conversely, knocking down *Cg25C* resulted in a strong reduction in Ndg^{AG3} localization and significant but not as drastic effects on the localization of Ndg^{AG1} and Ndg^{AG2} (Fig 6A and 6C). Altogether, these results show that localization directed by the G3 domain depends on Laminins, whereas localization by the G1 and G2 domains depends on Col IV.

Next we tested the ability of the Ndg mutant proteins lacking the G1, G2 or G3 domains, all three capable of localizing to BMs, to rescue the fat body BM defects observed in *Ndg*^l mutant larvae. Overexpression of the mutant variants Ndg^{AG1} or Ndg^{AG2} was able to rescue integrity of the fat body BM (Fig 6D), as imaged with *Cg25C*.RFP [53]. In contrast, expression of the mutant form Ndg^{AG3} failed to rescue BM integrity (Fig 6D), indicating that G3 is a key domain for Ndg function, while the G1 and G2 domains may function in a partially redundant way. This is supported by our results showing that *Ndg*^l/*Ndg*^{ARod-G3.1} transheterozygous mutant larvae show fat body BM defects indistinguishable from those found in *Ndg*^l homozygotes (Fig 4A and 4B).

The localization and rescue properties of the different domains of Ndg suggest that Ndg may indeed act as a linker between Laminin and Collagen IV, as originally proposed. Confirming this, simultaneous imaging of Collagen IV and Laminin in fat body BMs shows that in the *Ndg*^l mutant Laminin and Collagen IV appear separate from each other when the broken BM is observed at high magnification (Fig 6E; co-localization analysis in Fig 6G). Conversely, Perlecan and Collagen IV were still highly co-localized in the damaged BM of *Ndg* mutant fat body (Fig 6F and 6G). In all, these results are consistent with a function of Ndg as a linker of the Col IV and Laminin networks (Fig 6H). This linker function would depend on binding to Laminin through G3 and to Col IV through either G1 or G2.

Role of Laminins, Collagen IV and Perlecan in Nidogen incorporation into BMs

We have previously shown that *Drosophila* Laminins are critical for proper assembly of other ECM components in the BM of embryonic tissues [33]. Furthermore, a recent study has uncovered a temporal hierarchy of expression of BM components in the *Drosophila* embryo, with Laminins being expressed first, followed by Col IV and then Perlecan [30]. This seems to be critical for proper formation of the BM around the embryonic VNC. Thus, while elimination of Laminins affects both Col IV and Perlecan deposition, Laminin incorporates in the absence of any of these two components and Perlecan requires Col IV [30]. The requirements of these BM proteins for Ndg incorporation into embryonic BMs are still unknown. Here, we decided to investigate this by analysing Ndg expression in embryos devoid of the other BM components. We found that depletion of *LanB1* results in a strong reduction of Ndg accumulation in the gut, muscles and VNC (Fig 7A, 7A', 7B and 7B'). However, elimination of Col IV (Fig 7C and 7C') or Perlecan (Fig 7D and 7D') did not prevent Ndg deposition into embryonic BMs, except in the VNC midline pores of embryos lacking Col IV, where it is very much reduced.

Next, we tested the requirements of Laminins, Col IV and Perlecan for Ndg incorporation into the BM of the larval fat body. To this end, we analysed the expression of the transgene Ndg.sGFP in the fat body of larvae where we had knocked down expression of BM components under the control of *Cg*-GAL4 driver. We found that the knock down of Laminins or Col IV, but not Perlecan, caused a reduction in the amount of Ndg in fat body BMs (Fig 7E and 7F and S7 Fig), consistent with our functional analysis of the different Ndg domains (Fig 6).

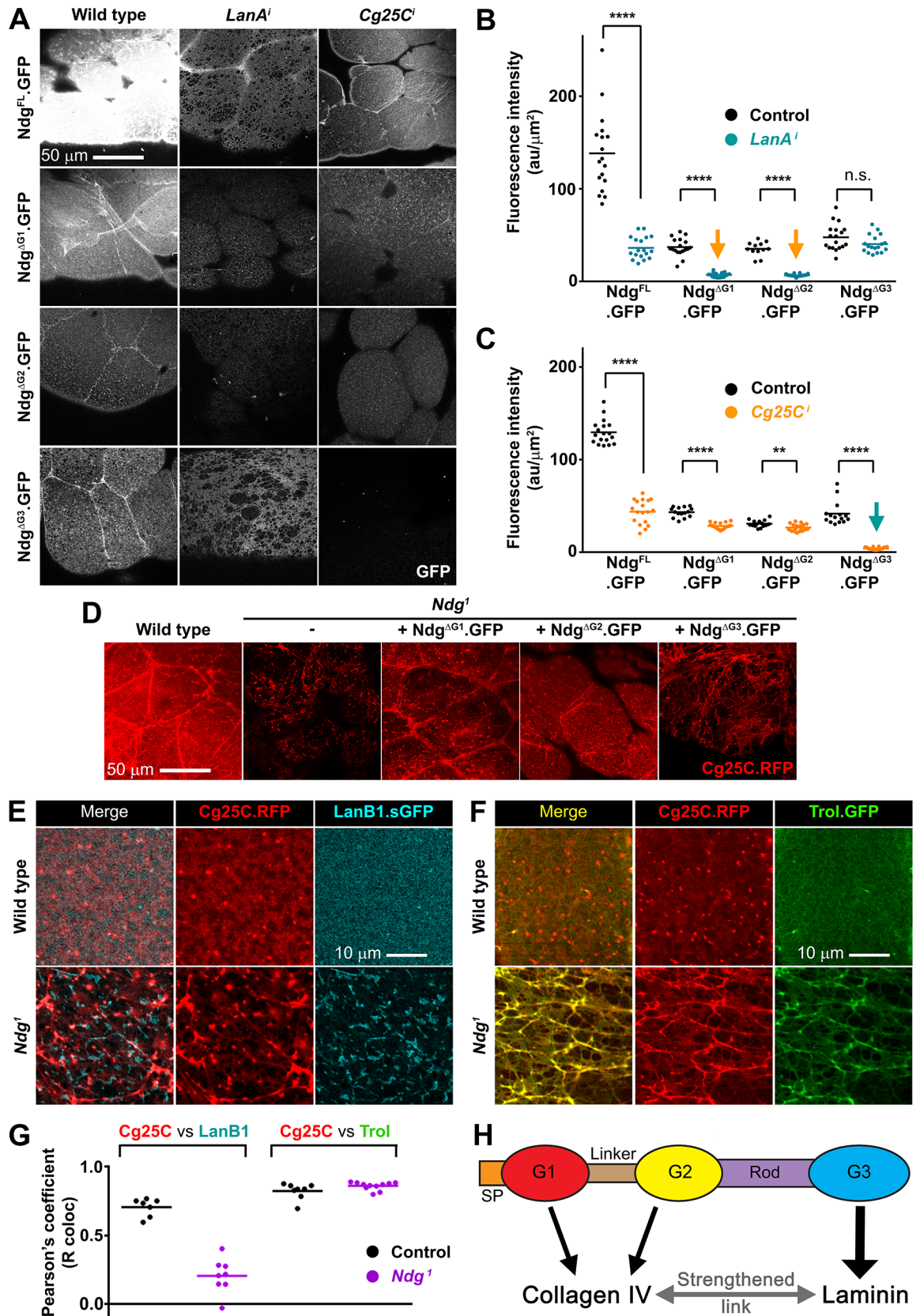


Fig 6. The G3 domain is essential for Ndg function. (A) Confocal images showing localization in fat body BM of the indicated GFP-tagged versions of Ndg, detected by GFP signal (white), in wild type (left column) and upon knock down of laminin (*Lana¹*, middle column) and Collagen IV (*Cg25C¹*, right column). (B, C) Quantification of GFP signal intensity of indicated GFP-tagged Ndg versions in the BM of wild type control, *Lana¹* (B) and *Cg25C¹* (C) fat body. Each dot represents a single measurement of intensity inside a 500 μm^2 square. Horizontal lines indicate the mean value (****: $p < 0.0001$; **: $p < 0.01$; n.s.: not significant). See [Materials and Methods](#) for statistical testing details. (D) Confocal images of the larvae fat body BM (*Cg25C.RFP* in red) in control, *Ndg¹* mutant, and *Ndg¹* mutant expressing *Ndg^{AG1}*, *Ndg^{AG2}* or *Ndg^{AG3}*. Integrity of the BM is restored by *Ndg^{AG1}* and *Ndg^{AG2}* but not *Ndg^{AG3}*. (E) Confocal images showing uncoupling of Collagen IV (*Cg25C.RFP* in red, middle panels) and Laminin (*LanB1.sGFP* in cyan, right panels) in *Ndg¹* mutant (lower panels) and wild type fat body (upper panels). Merged channels are shown in left panels. (F) Confocal images of Collagen IV (*Cg25C.RFP* in red, middle panels) and Perlecan (*Trol.GFP* in green, right panels) in *Ndg¹* mutant (lower panels) and wild type fat body (upper panels). Merged channels are shown in left panels. (G) Quantification of Pearson's colocalization coefficient after Costes thresholding (R colocalization) of Collagen IV with Laminin (E) and Collagen IV with Perlecan (F). (H) Model for the role of the G1, G2 and G3 domains on Ndg binding to Laminin and Collagen IV.

<https://doi.org/10.1371/journal.pgen.1007483.g006>

We additionally decided to analyze the mutual requirements of the remaining components of the adipose tissue BM. We found that loss of Col IV resulted in a strong reduction in Laminin levels and in a depletion of Perlecan (Fig 7E and 7F and S7 Fig). This is in agreement with previous results showing that knocking down *vkg* with *hsp70-GAL4*, which is a heat shock inducible promoter, reduced the presence of Nidogen and Laminin in fat body BM [54]. In contrast, and similar to the loss of Ndg (Fig 4), absence of Laminins led to holes in the BM without apparent reduction in Col IV or Perlecan levels (Fig 7E and S7 Fig). We also noted that reduction of Col IV and to a lesser extent of Laminins resulted in changes in adipocyte morphology and cell rounding. Finally, knock down of Perlecan did not affect the presence of any of the other components, consistent with the notion that it is a terminal BM component (Fig 7E and 7F) [29].

In summary, these results show that Ndg incorporation into embryonic and fat body BMs depends on both Laminin and Collagen IV. They also suggest a model for the assembly and maintenance of the adipose tissue BM in which Ndg is not essential for the incorporation of other components, but reinforces the connection between the Laminin and Col IV networks, thus allowing correct formation of the BM or preventing its rupture (Fig 7G).

Genetic interactions unmask a wider involvement of Nidogen in BM stability

To finally ascertain whether Nidogen incorporation had a wider stabilizing role on BMs despite limited phenotypic defects in the mutants, we tested genetic interactions with other conditions compromising BM functionality. *LanA²¹⁶* and *LanA¹⁶⁰* are two homozygous lethal EMS-induced *LanA* alleles that in combination produce animals viable until pupal stages [55]. While *LanA²¹⁶/LanA¹⁶⁰* 3rd instar larvae showed an elongated VNC, no defects in VNC condensation were observed in *LanA²¹⁶/+*, *LanA¹⁶⁰/+* or *Ndg¹* animals. In contrast, we found that *Ndg¹* mutants heterozygous for *LanA²¹⁶/+* or *LanA¹⁶⁰/+* showed VNCs that were significantly more elongated than those found in *Ndg¹ LanA²¹⁶/+* or *LanA¹⁶⁰/+* larvae (Fig 8A and 8B). In addition, we found that Ndg interacted genetically with Perlecan. Thus, while single knock down of either Ndg or Perlecan in the whole fly, using *actin-GAL4*, produced normal-looking pupae and viable adults, the double knock down of these genes caused a significant decrease in the size of pupae, which were unable to develop to adulthood (Fig 8C and 8D). This genetic interaction was exacerbated when knock down was driven at 30°C, a temperature at which *GAL4*-driven transgene expression is higher [56, 57]. In summary, these results prove that Nidogen interacts genetically with Laminins and Perlecan, suggesting a more general role of Nidogen in maintaining BM stability and consistent with its remarkable evolutionary conservation.

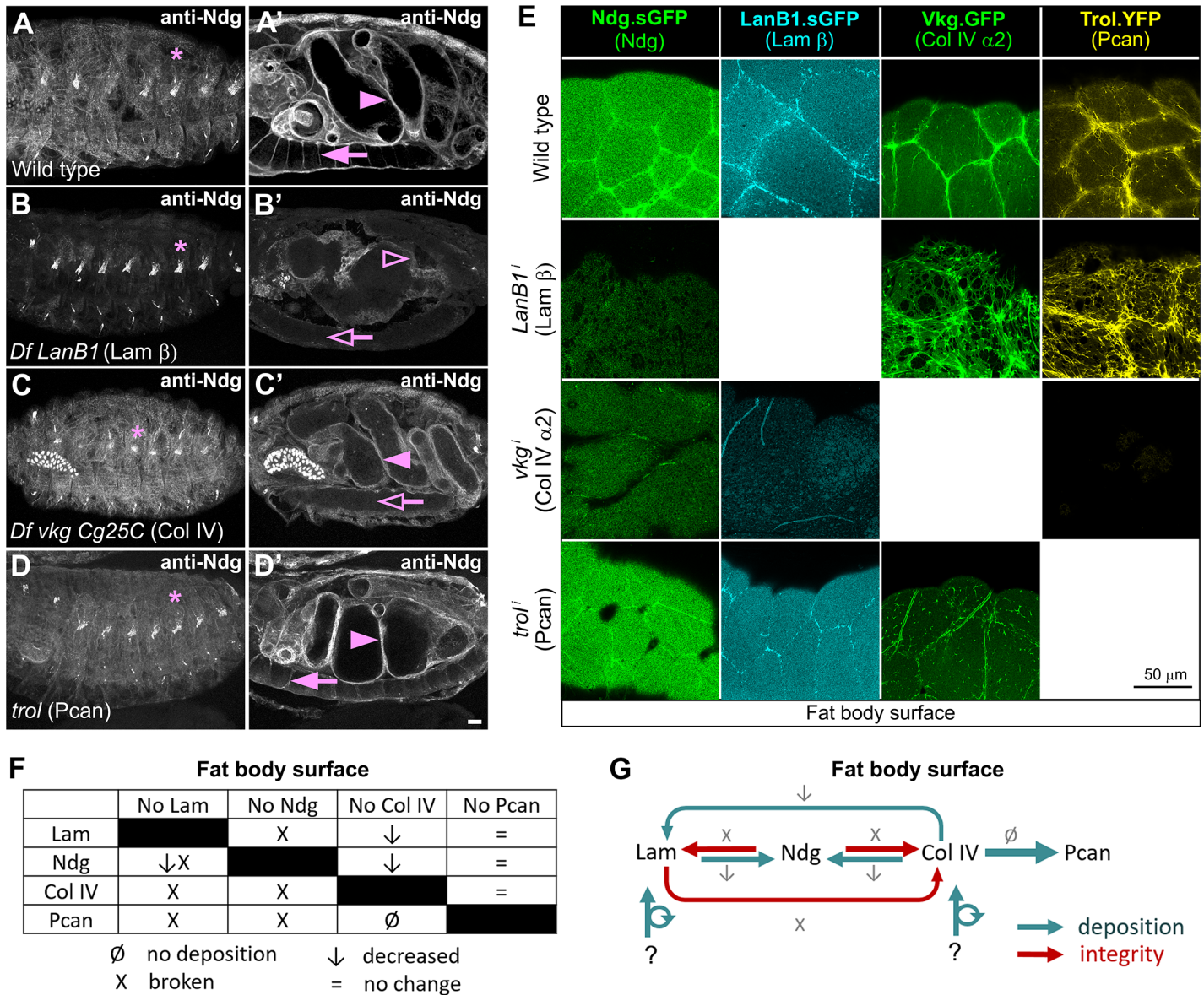


Fig 7. Laminins and Col IV are required for proper Ndg incorporation into adipose tissue BMs. (A-D') Confocal images showing stage 16 embryos stained with anti-Ndg. Images compare control embryos (A) with embryos depleted of the different BM components (B-D). (A-A') In control embryos, Ndg localizes to the BM of muscles (A), gut (A', arrowhead), VNC, midline pores (A', arrow) and in chordotonal organs (A, asterisk). (B) In Laminin-depleted embryos, Ndg is strongly reduced in the BM of muscles (B), gut (B', hollow arrowhead) and VNC (B', hollow arrow) and not affected in chordotonal organs (B, asterisk). (C-D) In contrast, Ndg deposition in these embryonic BMs is not affected in either Col IV (C-C') or Perlecan (D-D') mutant embryos, except for a reduction in Ndg in the midline pores in Col IV mutants (C', hollow arrow). Scale bar represents 20µm (A-D). (E) Confocal images of the fat body (adipose tissue) BM showing localization of Ndg (Ndg.sGFP, green), Laminin (LanB1.sGFP, cyan), Collagen IV (Vkg.GFP, green) and Perlecan (Trol.YFP, yellow). Images show fat body from wild type larvae (upper panels) and larvae where *LanB1*, *vkg* or *trol* have been knocked down using Cg-GAL4 (lower panels). (F) Table summarizing effects of the absence of each of the four major BM components on the other components in the BM of the fat body. (G) Model for the mutual relations of Laminin, Nidogen, Collagen IV and Perlecan in the BM of the fat body.

<https://doi.org/10.1371/journal.pgen.1007483.g007>

Discussion

BMs are thin extracellular matrices that play crucial roles in the development, function and maintenance of many organs and tissues [58]. Critical for the assembly and function of BMs is the interaction between their major components, Col IV, Laminins, proteoglycans and Ndg

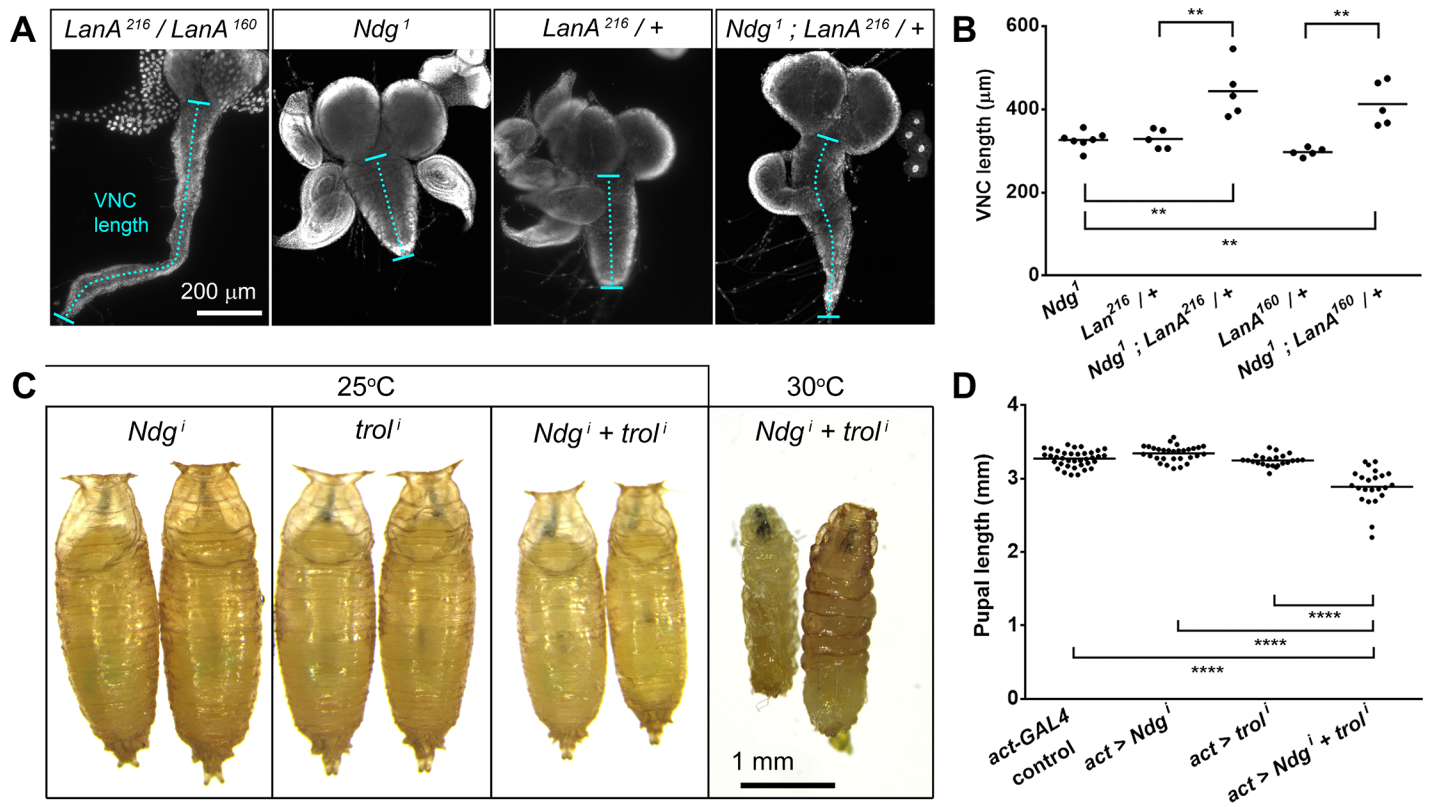


Fig 8. Ndg loss enhances Laminin and Perlecan loss phenotypes. (A) Larval ventral nerve cord (VNC) in *LanA²¹⁶/LanA¹⁶⁰*, *Ndg¹/Ndg¹*, *LanA²¹⁶/+* and *Ndg¹/Ndg¹; LanA²¹⁶/+* larvae. (B) Quantification of VNC length in *Ndg¹*, *LanA²¹⁶/+*, *Ndg¹; LanA²¹⁶/+*, *LanA¹⁶⁰/+* and *Ndg¹; LanA¹⁶⁰/+*. Each dot represents an individual VNC measurement. Horizontal lines indicate the mean value. Differences with the control were significant in non-parametric Mann-Whitney tests (**; $p < 0.01$). (C) Images of pupae where *Ndg*, *trol* or both *Ndg* and *trol* have been knocked down using act-GAL4 at either 25°C or 30°C. (D) Quantification of pupal length in wild type control, *act>Ndgⁱ*, *act>trolⁱ* and *act>Ndgⁱ+trolⁱ* pupae. Each dot represents a single pupa measurement. Horizontal lines indicate the mean value. Differences with the control were significant in non-parametric Mann-Whitney tests (****; $p < 0.0001$).

<https://doi.org/10.1371/journal.pgen.1007483.g008>

[59]. Both the ability of Ndg to bind laminin and Col IV networks and the crucial requirements for Laminins and Col IV in embryonic development [60, 61] anticipated a key role for Ndg during morphogenesis. However, experiments showing that elimination of Ndg in mice and *C. elegans* are compatible with survival casted doubt upon the crucial role for Ndg in organogenesis as a linker of the crucial Laminin and Col IV networks within the BM. Here, we have isolated mutations in the single *Drosophila* *Ndg* gene and found that, as it is the case in mammals and *C. elegans*, *Ndg* is not generally required for BM assembly and viability. However, *Ndg* mutant flies display mild motor or behavioral defects. In addition, similar to mammals, we show that the Nidogen-deficient flies show BM defects only in certain organs, suggesting tissue-specific roles for *Ndg* in BM assembly and maintenance. Finally, our functional study of the different *Ndg* domains challenges the significance of some interactions derived from in vitro experiments while confirming others and additionally revealing a new key requirement for the Rod domain in *Ndg* function and incorporation into BMs.

Results from cell culture and in vitro experiments led to propose a crucial role for *Ndg* in BM assembly and stabilization. Recombinant *Ndg* promotes the formation of ternary complexes among BM components [62]. In addition, incubation with recombinant *Ndg* or antibodies interfering with the ability of *Ndg* to bind Laminins results in defects in BM formation and epithelial morphogenesis in cultured embryonic lung, submandibular glands and kidney [63, 64]. However, elimination of *Ndg* in model organisms has shown that *Ndg* is not essential

for BM formation per se but required for its maintenance in some tissues. Thus, while the early development of heart, lung and kidney prior to E14 is not affected in Nidogen-deficient mice, defects in deposition of ECM components and BM morphology were observed at E18.5 [11]. Similarly, whereas BM components localized normally in Nidogen-deficient mice during the early stages of limb bud development, this BM breaks down at later stages [12]. In contrast, removal of *Ndg* does not impair assembly or maintenance of any BM in *C. elegans* [14]. Here, we show that in *Drosophila*, as it is the case in mammals [11, 12], different BMs have different requirements for *Ndg*. Thus, while elimination of *Ndg* in *Drosophila* does not impair embryonic BM assembly or maintenance, it results in discontinuity of the BM in fat body and flight muscles. The basis for this tissue-specificity of *Ndg* requirements is currently unknown. Recent experiments have shown that there is a tissue-specific hierarchy of expression and incorporation of BM proteins in the *Drosophila* embryo, with Laminins being expressed first followed by Col IV and finally Perlecan [30]. Laminins and Col IV can reconstitute polymers in vitro that resemble the networks seen in vivo [32] [65]. In this context, Laminins and Col IV could self-assemble into networks in the embryo as they are produced, being this sufficient to assemble a BM capable of sustaining embryonic development in the absence of the two subsequent components, *Ndg* and Perlecan. We also show here that, while fat body and blood cells are the source of the majority of the proteins in larval BMs, there are notable exceptions, a fact that highlights a diversity in the origins of BM components in different tissues. Thus, fat body produces entirely all its BM, the larval heart receives it all from the hemolymph, imaginal discs produce a portion of their Laminins and similarly for tracheae with respect to Perlecan. These differences in the source of BM components for different tissues (incorporated vs. self-produced) may impose different assembly mechanisms, a possibility to study in more detail in the near future. In addition, although BM components are universally present in numerous tissues and organs, they are diverse depending on tissue and developmental stage (reviewed in [66]). This heterogeneity arises from variations in protein subtypes, such as the two alternative Laminin α chains or the numerous Perlecan isoforms. Heterogeneity may also stem from differences in relative amounts of each component and posttranslational modifications thereof. In this respect, it is possible that BM assembly of the *Drosophila* fat body and adult flight muscles of the notum is such that is more dependent on *Ndg* function for its formation and stability than BMs found in other tissues. Finally, dynamics of BMs can orchestrate organ shape changes. Reciprocally, the associated tissues can control properties of BMs by, for instance, expressing a specific repertoire of ECM receptors or remodeling factors. In this context, it is also possible that fat body or adult flight muscles sculpt BMs with properties demanding a high requirement of *Ndg* function.

We find here that *Ndg* mutant flies are less fertile and behave differently with respect to wild type in ChillComa Recovery Time assays. The physiological mechanisms underlying the response in insects to critical thermal limits remain largely unresolved. The onset and recovery of chill coma have been attributed to defects in neuromuscular function due to depolarization of muscle fiber membrane potential [67]. Interestingly, flight muscle fiber membrane is strongly depolarized upon exposure to low temperatures in *Drosophila* [67]. In this context, the defects we observed in the BM of adult flight muscles in the absence of *Ndg* could be behind the defective response of *Ndg* mutant flies to chill coma recovery assays. Altogether, these results show that, though not critical for survival, *Ndg* is required for overall fitness of the fly.

All Nidogen proteins consist of three globular domains, G1 to G3, and two connecting segments, one Rod domain separating G2 and G3 and a flexible linker between G1 and G2. Crystallographic and binding epitope analyses using recombinant domains of the mouse Nidogen-1 protein have demonstrated high affinity binding of domain G2 to Col IV and Perlecan, of

domain G3 to the Laminin γ 1 chain and Col IV, and no activity for the Rod domain [4–7, 68]. In addition, recent physicochemical studies analyzing the solution behavior of full length purified Nidogen-1 confirmed the formation of a high affinity complex between the G3 domain of Nidogen-1 and the Laminin γ 1 chain, and excluded cooperativity effects engaging neighboring domains of both proteins [69]. However, little is known about the functional meaning of the binding abilities of Ndg on its localization and function in BM assembly in vivo. In fact, mutant *C. elegans* animals carrying a deletion removing the entire G2 domain of NID-1 are viable and show no defects on Ndg or Col IV localization in BMs [14]. These results demonstrate that, despite the strong sequence conservation between *C. elegans* and mammalian G2 domains, *C. elegans* NID-1 localization appears to occur independently of this domain. Here, we show that, as it is the case in *C. elegans*, the *Drosophila* G2 domain is not essential for neither Ndg localization nor function. A possible explanation for this result is that although some of the modules present in BM components are conserved, there might be variations in sequence and structure that might be sufficient to confer binding specificity to the different proteins. For instance, the IG3 domain of mouse Perlecan, which binds to a β -barrel in the G2 domain of Nidogen, is strikingly conserved in all mammals, but not in *Drosophila* or *C. elegans* [70, 71]. This result suggests that either the Perlecans present in these organisms are too distant in evolution from the mouse proteins for these domains to be conserved or that Perlecans may only bind Nidogen in mammals. Previous studies aimed to characterize the biological significance of the Nidogen-Laminin interactions have targeted the Nidogen-binding module of the Laminin γ 1 chain, showing that this domain is required for kidney and lung organogenesis [63] [72]. However, the role of the Nidogen G3 domain has not yet been addressed directly. Here, we show that the G3 domain is essential for Ndg localization, supporting a role for Nidogen-Laminin interactions on Ndg function. In addition, in contrast to what has been shown in mammals (see above), our results unravel a key role for the Rod domain in Nidogen localization. Again, an explanation for this result could hinge on variations in Nidogen between species. In fact, one of the major differences between *Drosophila* and mammalian Nidogen lies on the Rod domain. Thus, while vertebrates have four EGF repeats and one or two thyroglobulin repeats, *Drosophila* and *C. elegans* have 12 and 11 EGF repeats, respectively. Alternatively, conclusions derived from in vitro studies may not be always applicable to the circumstances occurring in the living organism. Furthermore, the appearance of new in vitro studies combining different techniques has revealed the existence of multiple Nidogen-1/Laminin γ 1 interfaces, which include, besides the known interaction sites, the Rod domain [68].

Different BM assembly models have been proposed over the last thirty years. Based upon biochemical studies and rotary shadow electronic microscopic visualization, the BM assembly model firstly proposed that Collagen IV self-assembles into an initial scaffold, followed by Laminin polymerization structure attachment mediated by Perlecan [73, 74]. However, more recent studies have postulated a contradicting model for in vivo systems. The most widely endorsed model states that the polymer structure is initiated by a Laminin scaffold built through self-interaction, bridged by Nidogen and Perlecan and finally completed by another independent network formed by Col IV self-interaction [4]. Here, we studied in detail the hierarchy of BM assembly in the *Drosophila* larval fat body. Thus, while the requirements for *Drosophila* Laminins in the incorporation of other ECM components into BMs are preserved between tissues, this is not the case for Collagen IV. For instance, absence of Col IV does not completely prevent deposition of Laminin in the fat body, but remarkably reduces it (Fig 7E); in contrast, no such drastic effect has been observed in wing discs or embryonic BMs [29, 30], suggesting that Collagen IV does not affect Laminin incorporation in these other tissues to the same degree or that it does not affect it at all. In addition, we found that BM assembly in *Drosophila* also differs from that in mammals and *C. elegans*. In this case, the divergences may

arise during evolution, when different organisms might have incorporated novel ways to assemble ECM proteins to serve new specialized functions.

Nidogen has been proposed to play a key role in BM assembly based on results from in vitro experiments and on its ability to serve as a bridge between the two most abundant molecules in BMs: Laminin and Type IV Collagen. However, phenotypic analysis of its knock out in mice and *C. elegans* have called into question a general role for Nidogen in BM formation and maintenance. Here, we show that although Ndg is dispensable for BM assembly and preservation in many tissues, it is absolutely required in others. These differences on Ndg requirements stress the need to analyze its function in vivo and in a tissue-specific context. In fact, we believe this should also be the case when analyzing the requirements of the other ECM components for proper BM assembly, as we show here they also differ between species and tissues. One has to be cautious when inferring functions of different BM proteins or their domains based on experiments performed in vitro or in a tissue-specific setting. This might be especially relevant when trying to apply conclusions derived from these studies to our understanding of the pathogenic mechanisms of BM-associated diseases or to the development of innovative therapeutic approaches.

Materials and methods

Fly strains

Standard husbandry methods and genetic methodologies were used to evaluate segregation of mutations and transgenes in the progeny of crosses [75]. The following stocks were used:

The FTG, CTG and TTG balancer chromosomes, carrying twist-Gal4 UAS-2EGFP, were used to identify homozygous *Ndg*^{ARod-G3} mutants [76]. For the generation of Ndg deficiencies the following stocks were used (all from Bloomington *Drosophila* Stock Center): *Mi{ET1}* *Ndg*^{MB12298}, *w*; *BlmN1/TM3*, *Sb1* [77], *w*; *Sco/Sm6aP(hsILMit)2,4*, *w*; *Gla/CyO*, *Df(2L)BSC172* [29] and *Df(2R)BSC281*.

w; *tub-GAL80^{ts}*, *y v*; *UAS-trol.RNA*^{TRiP.JF03376}, *y v*; *Ndg.RNAi*^{TRiP.HMJ24142}, *y v sc*; *UAS-LanB2.RNAi*^{TRiP.HMC04076}, *y v*; *UAS-LanA.RNAi*^{TRiP.JF02908}, *w*; *UAS-GFP.S65T* (BDSC 1522), *w*; *en2.4-GAL4 UAS-mCherry.NLS* (BDSC 38420) and *y v sc*; *UAS-EGFP.shRNA* (BDSC 41560) are from Bloomington *Drosophila* Stock Center. *w*; *Ndg.sGFP*^{TRG.638}, *w*; *LanB1.sGFP*^{TRG.638}, *w*; *UAS-LanB1.RNAi*^{VDRC.v23121}, *w*; *UAS-trol.RNAi*^{VDRC.v24549} and *w*; *UAS-Cg25C.RNAi*^{VDRC.v28369} were obtained from Vienna *Drosophila* Resource Center. *y w*; *vkg*^{G454}.GFP, *w* *trol*^{ZCL1700}.GFP and *w* *trol*^{CPTI-002049}.YFP were from *Drosophila* Genomics Resource Center. *w*; *UAS-vkg.RNAi*^{NIG.16858R-3} was from National Institute of Genetics.

Other strains used were: *Df LanB1/CTG* [33], *Df(3R)BSC524/CTG* [78], *trol*^{null}/FMZ [79], *w*; *UAS-Cg25C.RFP3.1* [45] and *croc-lacZ* [42]. *w*; *LanA*¹⁶⁰/TM6B, and *w*; *LanA*²¹⁶/TM6B are gifts from Luis Garcia-Alonso. *w*; *UAS-secreted.GFP* is a gift from Fujian Zhang.

Lines generated in this study are: *w*; *sGFP*^{RNAi}.attP40, *w*; *Ndg*¹, *w*; *Ndg*², *Ndg*^{ARod-G.3.1}, *Ndg*^{ARod-G.3.2}, *Ndg*^{ARod-G.3.3}. *w*; *UAS-Ndg*^{FL}.GFP, *w*; *UAS-Ndg*^{G1}.GFP, *w*; *UAS-Ndg*^{G2}.GFP, *w*; *UAS-Ndg*^{G3}.GFP, *w*; *UAS-Ndg*^{Rod}.GFP, *w*; *UAS-Ndg*^{RodG3}.GFP, *w*; *UAS-Ndg*^{G1L}.GFP, *w*; *UAS-Ndg*^{G1LG2}.GFP, *w*; *UAS-Ndg*^{AG3}.GFP, *w*; *UAS-Ndg*^{AG2R}.GFP, *w*; *UAS-Ndg*^{AG2}.GFP, *w*; *UAS-Ndg*^{AG1}.GFP, *w*; *UAS-Ndg*^{G2R}.GFP, *w*; *UAS-Ndg*^L.GFP and *w*; *UAS-Ndg*^{AR}.GFP.

The description of all lines used in this study is available in Supplementary information S2 Table.

The GAL4-UAS system was used to drive expression of transgenes and RNAi constructs in larval fat body and hemocytes (blood cells) under control of Cg-GAL4 (BDSC 7011) or BM-40-SPARC-GAL4 (gift from Hugo Bellen), and ubiquitously with act-GAL4.

For Collagen IV knock down experiments (*vkgⁱ* and *Cg25Cⁱ*), thermosensitive GAL4 repressor GAL80^{ts} was used to prevent embryonic lethality. Cultures were grown at 18°C for 6 days, followed by transfer of cultures to 30°C (L2 stage) and dissection two days later (L3 stage).

Transgenic flies

sGFP RNAi. Short hairpin oligoes to knock down sGFP were designed following instructions in DSIR website (<http://biodev.extra.cea.fr/DSIR/DSIR.html>) [80].

Top strand oligo: CTAGCAGTAGCTGGAGTACAACCTCAACATAGTTATATTCAAGCATATGTTGAAGTTGTAAGTCCAGCTGCG.

Bottom strand oligo: AATTCGCTGTTGAAGTTGTAAGTCCAGCTTATGCTTGAATATAACTAAGCTGGAGTACAACCTCAACAACCTG.

After annealing the top and bottom strand oligoes, the product was inserted into the VAL-IUM22 vector, which had been previously linearized by NheI and EcoRI double restriction (New England Biolabs, Ipswich, Massachusetts). The resulting plasmids were transformed, miniprepmed with QIAprep Spin Miniprep Kit (QIAGEN, Hilden, Germany) and injected into fly strain *y sc v nanos-integrase; attP40* for stable transgene integration [81].

UAS-Ndg^{FL}.GFP. The coding sequence of Nidogen was amplified by PCR from 3rd instar larval cDNA with forward primer: GGGGACAAGTTTGTACAAAAAAGCAGGCTTCATGCGACCTTCGGCAGTAAGTTGC and reverse primer:

GGGGACCACTTTGTACAAGAAAGCTGGGTC GTAGCCAGGCGCCAGCACGG.

The resulting product was cloned into PDONR211 (Life Technologies, Carlsbad, California) using Gateway BP Clonase Enzyme Mix (Life Technologies) to obtain PDONR211-Ndg, which was finally transferred into destination vector PTWG-1076 (UAST C-terminal GFP, *Drosophila* Carnegie Vector collection) plasmid by using Gateway LR Clonase Enzyme Mix (Life Technologies). Transgenic lines were obtained through standard P-element transgenesis [82].

Other Nidogen constructs

For the structure/function analysis of Ndg domains, deletion of specific domains of Ndg was achieved by PCR-amplifying plasmid PDONR211-Ndg with the appropriate combinations of the following primers:

Ndg^{G1}.GFP-Forward: TGAGAACGAGGACCCAGCTTTCTTGTACAAAG

Ndg^{G1}.GFP-Reverse: AAGCTGGGTCCTCGTTCTCAATGGGAGCCAC

Ndg^{G2}.GFP-Forward: GGTCAGCGGAGCTAATGATCAACCTATCCGAGTG

Ndg^{G2}.GFP-Reverse: GATCATTAGCTCCGCTGACCAGGATCACCCGAG

Ndg^{G3}.GFP-Forward: CAGCGGACAGCGTCCCATTTCGGTGGCCC

Ndg^{G3}.GFP-Reverse: AAATGGGACGCTGTCCGCTGACCAGGATCAC

Ndg^{Rod}.GFP-Forward: GACATTACGTGACCCAGCTTTCTTGTAC

Ndg^{Rod}.GFP-Reverse: AAGCTGGGTCGACATTACGTCCGTTTAG

Ndg^{RodG3}.GFP-Forward: GGTCAGCGGAAACGATGGTACCGCCGATTG

Ndg^{RodG3}.GFP-Reverse: TACCATCGTTTCCGCTGACCAGGATCACCCGAG

Ndg^{G1L}.GFP-Forward: GTCCTGCCTGTACGACCCAGCTTTCTTGTACAAAG

Ndg^{G1L}.GFP-Reverse: CTGGGTCGTACAGGCAGGACTTTCCATTGCC

Ndg^{G1LG2}.GFP-Forward: AAATGGGACGCAGGCAGGACTTTCCATTGCC

Ndg^{G1LG2}.GFP-Reverse: CTGGGTCGTAATCGTTGCAGGCATTTCGATTCCGG

Ndg^{AG3}.GFP-Forward: GACATTACGTGACCCAGCTTTCTTGTAC

Ndg^{AG3}.GFP-Reverse: AAGCTGGGTCGACATTACGTCCGTTTAG

Ndg^{AG2R}.GFP-Forward: GTCCTGCCTGCGTCCCATTTCGGTGGCCCAG

Ndg^{AG2R}.GFP-Reverse: AAATGGGACGCAGGCAGGACTTTCCATTGCC
 Ndg^{AG2}.GFP-Forward: GTCCTGCCTGAACGATGGTACCGCCGATTG
 Ndg^{AG2}.GFP-Reverse: TACCATCGTTCAGGCAGGACTTTCCATTGCC
 Ndg^{AG1}.GFP-Forward: GGTCAGCGGAGAGCAGAACGTGAGGTCTCCC
 Ndg^{AG1}.GFP-Reverse: CGTTCTGCTCTCCGCTGACCAGGATCACCGAG
 Ndg^{G2R}.GFP-Forward: GGTCAGCGGAGCTAATGATCAACCTATCCG
 Ndg^{G2R}.GFP-Reverse: GATCATTAGCTCCGCTGACCAGGATCACCG
 Ndg^L.GFP-Forward: GGTCAGCGGAGAGCAGAACGTGAGGTCTCC
 Ndg^L.GFP-Reverse: CGTTCTGCTCTCCGCTGACCAGGATCACCG
 Ndg^{AR}.GFP-Forward: GAATGCCTGCCGTCCCATTTGCGGTGGCCCA
 Ndg^{AR}.GFP-Reverse: AAATGGGACGCGCAGGCATTTCGATTCCGGGG

The resulting PCR reactions were incubated with 10 units of DMT enzyme (TransGen Biotech, Beijing, China) at 37°C for 1 hour to digest the original templates. After digestion, PCR products were transformed into DMT competent cells (TransGen Biotech, Beijing, China). Colonies were validated by sequencing. Transgenic lines were obtained through standard P-element transgenesis [82].

Generation of deficiencies removing the gene Ndg

The Mi{ET1}Ndg^{MB12298} transposon was used in a Blm mutant background to generate deficiencies by imprecise excision of the transposon. In these mutants, homologous recombination DNA repairing enzymes are compromised, thus increasing the events of non-homologous recombination DNA repair. Non-homologous recombination DNA repair increases the chances of generating DNA deficiencies [77]. We selected 132 Blm mutant males carrying the Mi{ET1}Ndg[MB12298] transposon and crossed them to w; Gla/CyO females. The offspring of this cross rendered a 110 EGFP negative males that were crossed to the Df(2R)BSC281 deficiency. 6 out of the 110 males did not complement the deficiency and were selected for further molecular characterization with the following primers from the Ndg genomic region. PCR primers were used as follows: (5'-3')

Ndg primer1-Forward: GTGTGGACTCGGTGTGACTG
 Ndg primer1-Reverse: ACTTCGAACAGCCAGACTCC
 Ndg primer2-Forward: CCTTCGGCAGTAAGTTGCTC
 Ndg primer2-Reverse: GTGCTGTTGGACAGACAACG
 Ndg primer3-Forward: CGATCAAGCGGCGCAATATC
 Ndg primer3-Reverse: CCAACATGCCACAATGGGTG
 Ndg primer4-Forward: GTCTGAGTGGTTTCGGCAC
 Ndg primer4-Reverse: TTTGCTTAAAGTGGGTGTTGC
 Ndg primer5-Forward: CCATTGTGGCATGTTGGATA
 Ndg primer5-Reverse: TGTTTCGAAGGCGATACTCA
 Ndg primer6-Forward: AAAGTGAAGGCGGGGAAT
 Ndg primer6-Reverse: TTAATCAGTGCACCGCAGAG
 Ndg primer7-Forward: GATGAAGGAGGCAAAGCAAAG
 Ndg primer7-Reverse: TTTTCATCTGCAGTGCCTTC
 Ndg primer8-Forward: GAGGAGCAGATACCCCAACA
 Ndg primer8-Reverse: CAGTGCCGTCATATTTGGTG
 Ndg primer9-Forward: GGATTCAGAGGCGATGGATA
 Ndg primer9-Reverse: GACCAGTTCCGTCCAGGTTA
 Ndg primer10-Forward: TTTCTGCCAGTTTTCGCTTT
 Ndg primer10-Reverse: CGTGTTGTTGGATTGTGGAG

Ndg primer11-Forward: GTGCTGTGCCTCAGATGAAA

Ndg primer11-Reverse: GGGAACCCAATGTGCTTAGA

Ndg primer12-Forward: TTACCTTCACGCACGATCAG

Ndg primer12-Reverse: GGCTGCGGCATTAGAGATAC

All deficiencies eliminated the 5' UTR and the first exon of the *Ndg* gene and at least two adjacent genes: *Obp46a* and *CG12909* (S2 Fig).

Generation of *Ndg* mutants with CRISPR/Cas9

Four sgRNAs were designed for generating *Ndg* null mutant lines [83]. sgRNAs and cas9 mRNA were injected into *w¹¹¹⁸* embryos. *Ndg* deletions in the germ line *Ndg¹* and *Ndg²* were selected by sequencing by Beijing Fungene Biotechnology (Beijing, China).

sgRNA1: GAGAGATACACAAGTCAGGAAGG

sgRNA2: CCAGCCCTTCCGCTGGAATATGC

sgRNA3: GCGGCCTTCTACTCGAACGTGG

sgRNA4: GCCATTTGCAAGTGGGACTCGG

For assessment of *Ndg* mRNA expression in *Ndg¹* mutants was assessed by quantitative real-time PCR. RNA was extracted using TRIzol reagent (Life technologies, USA). cDNA was synthesized from 2 µg of RNA with PrimeScript RT-PCR Kit (Takara, Kyoto, Japan). Analysis was performed in a CFX96 Touch system (Bio-Rad, California, USA) using iTaq Universal SYBR Green Supermix (Bio-Rad). *rp49* was used as a reference for normalization. Three experiments per genotype were averaged. The following intron-spanning pairs of primers were used:

Ndg primerA-Forward: GAGCAGTACGAGCAGCT

Ndg primerA-Reverse: CGAGTAGAAGGCCGCTAT

Ndg primerB-Forward: ATCCATATCCTGAGGAGCAGAT

Ndg primerB-Reverse: GGTGCAGGTGTAGCCAT

Ndg primerC-Forward: AGTGCCGTTGACCAATT

Ndg primerC-Reverse: GACAATCAGGAAGTCAGAGT

Ndg primerD-Forward: GACTCAGCAAAGGATACCAT

Ndg primerD-Reverse: CAGTCCGACCAGAACAGTT

rp49 primer-Forward: GGCCCAAGATCGTGAAGAAG'

rp49 primer-Reverse: ATTTGTGCGACAGCTTAGCATATC

To generate *Ndg* mutants carrying a deletion of the rod and G3 domains, one single guide (sgRNA) target was designed in the 5th exon of *Ndg*:

sgRNA5: GGGGAATGCCGATGCCCCCTATGG

The sgRNAs were cloned in the PCFD3 vector as previously described in [84] and <http://www.crisprflydesign.org/plasmids/>. Transgenic gRNA flies were created by the Best Gene Company (Chino Hills, USA) using either *y sc v P{nos-phiC31\int.NLS}X; P{CaryP}attP2* (BDSC 25710) or *y v P{nos-phiC31\int.NLS}X; P{CaryP}attP40* (BDSC 25709). Transgenic lines were verified by sequencing by Biomedal Company (Armill, Spain). Males carrying the sgRNA were crossed to females either act-Cas9 or nos-Cas9 and the progeny was screened for the v+ch- eye marker. To identify CRISPR/Cas9-induced mutations, genomic DNA was isolated from flies and sequenced using the following primers: (5'-3')

Ndg primerg5-Forward: GCGAAGTTTGGGAGAACGGA

Ndg primerg5-Reverse: ACAGTATCTCACTCAGATCGGC

Immunohistochemistry and imaging

For generation of anti-Nidogen antibody, rabbits were immunized with epitope CTYVQ EFDGERNADLIPC by Bio-med Biotechnology (Beijing, China). Embryos, fat bodies, wing

imaginal discs and ovaries were stained using standard procedures and mounted in DAPI-Vectashield (Vector Laboratories, Burlingame, California). The following primary antibodies were used: rabbit anti-Ndg (1:2000, this study), chicken anti-beta-galactosidase (1:500, AbCam, Cambridge, UK), chicken anti-GFP (1:500, AbCam), rabbit anti-Ndg (1:100, [34]). Secondary antibody is IgG conjugated to Alexa-555, IgG conjugated to Alexa-488 and Alexa 549 (1:200, Life technologies).

For lipid droplet staining, L3 larvae were turned inside out and fixed in 4% PFA for 20 minutes, washed twice in PBS and then incubated in a 1:1000 dilution in PBS of 1 mg/ml BODIPY 493/503 stock (Life Technologies) for 30 minutes, followed by two 10-min washes in PBS and mounting in DAPI-Vectashield (Vector Laboratories). Confocal images were obtained using a Leica (Wetzlar, Germany) SP2 microscope or a Zeiss (Oberkochen, Germany) LSM780 microscope equipped with a Plan-Apochromat 63X oil objective (NA 1.4). Eggs and pupae were imaged in a Leica M125 stereoscope. All images were processed with Adobe Photoshop and ImageJ.

Quantification

For quantification of lipid droplet diameter (Fig 4E), confocal micrographs of 3rd instar larval fat body stained with BODIPY were analyzed with the automated particle detection tool of Nikon NIS-Elements AR 5.0 software. Sixteen adipocytes per genotype were analyzed and only particles larger than 3 μm in diameter were counted. For quantification of egg laying (S4A Fig), five 2-day old virgins were transferred to fresh vials daily for ten days and the eggs laid on each vial counted. Three such experiments were conducted per genotype.

For calculation of egg aspect ratio (S4B Fig; [85]) length and width of eggs were measured on images using the line tool in FIJI-ImageJ. Aspect ratio is defined as egg length divided by width.

In chill coma recovery time assays (S4D Fig; [51]), 2-day old females were placed into 10 mL tubes. These tubes were submerged into an ice-water bath for 2 hours, resulting in paralyzed flies. The amount of time required for a fly at room temperature to stand after becoming paralyzed in this way was measured.

For quantification of fluorescence intensity of different Ndg.GFP constructs in fat body BM (Fig 6B and 6C), GFP signal was measured on 4–6 confocal images per genotype using FIJI-ImageJ. Each measurement represents mean value intensity inside a 500 μm^2 square drawn on a flat portion of BM of an individual fat body cell, avoiding measuring intensity in cell contacts.

For colocalization analysis (Fig 6G), 63x confocal images of fat body were analyzed. Pearson's correlation coefficients after automated Costes thresholding (R coloc) were calculated with the FIJI-ImageJ plugin Colocalization Threshold. Each data point in the graph represents one image containing several fat body cells, like those in Fig 6D. VNC length (Fig 8B) was measured on confocal images using the segmented line tool of FIJI-ImageJ.

For quantification of pupal length (Fig 8D), stereoscope images of pupae were measured using the line tool of FIJI-ImageJ. Each data point in the graph represents one pupa.

Statistical analysis

Graphpad Prism software was used for graphic representation and statistical analysis. For measurements of lipid droplet diameter (Fig 4E), a non-parametric Mann-Whitney test was used. For statistical comparisons of fluorescence intensity in Fig 6B and 6C, unpaired Student's t tests were used in $LanA^i+Ndg^{AG3}.GFP$, $Cg25C^i+Ndg^{FL}.GFP$, $Cg25C^i+Ndg^{AG1}.GFP$ and $Cg25C^i+Ndg^{AG2}.GFP$ experiments (data passed D'Agostino & Pearson normality tests and F-tests for

equal variance). Student's t tests with Welch's correction were used for *LanAⁱ+Ndg^{FL}.GFP*, *LanAⁱ+Ndg^{AG1}.GFP* and *LanAⁱ+Ndg^{AG2}.GFP* experiments (data passed D'Agostino & Pearson normality tests, but not F-tests for equal variance). A non-parametric Mann-Whitney test was used in *Collagen IVⁱ+Ndg^{AG1}.GFP* experiment (data did not pass D'Agostino & Pearson normality test). For comparisons of VNC length in Fig 8B and pupal length in Fig 8D, we performed non-parametric Mann-Whitney tests. For egg production curves in S4A Fig, we conducted non-parametric Kolmogorov-Smirnov tests. For comparison of aspect ratio in S4B Fig, we performed unpaired two-tailed Student's t tests. For comparison of chill coma recovery time in S4C Fig, Student's t-tests with Welch's correction were used. Significance of statistical tests is reported in graphs as follows: **** ($p < 0.0001$), *** ($p < 0.001$), ** ($p < 0.01$), * ($p < 0.05$), n.s. ($p > 0.05$).

Supporting information

S1 Fig. Fat body adipocytes and blood cells are the main source of BM components in the larva. (A) Confocal images showing the localization of Collagen IV (Vkg.GFP, green), Perlecan (Trol.YFP, yellow) and Laminin (LanB1.sGFP, cyan) in different tissues of the 3rd instar larva. Images compare control tissues (+) with tissues from larvae where expression of the corresponding fluorescence protein fusion has been knocked down through Cg-GAL4-driven iGFPi (*Cg>isGFPi*). Disappearance of the corresponding signal from BMs is observed, with the exceptions indicated by hollowed arrows (partial reduction) and asterisks or filled arrows (no reduction). Nuclei stained with DAPI (white). (B) LanB1.sGFP signal (cyan) in the posterior compartment of the wing disc is reduced in *en>LanB1ⁱ* larva. Posterior compartment cells (*en+*) express mCherry (red). (TIFF)

S2 Fig. Generation of deletions removing the Ndg gene. (A) Schematic representation of the deficiencies generated in the Ndg region by imprecise excision of the Mi{ET1}Ndg[MB12298] transposon (see Materials and Methods). (B) Colour-code diagram picture of the primer pairs used for molecular characterization of the deficiencies described in (A) (see Materials and Methods). (TIF)

S3 Fig. Ndg accumulation in *Ndg^{ARod-G3.1}* homozygous mutant embryos. (A-D) Confocal images showing stage 16 embryos stained with two different anti-Ndg (red) antibodies. Images compare control embryos (A) with *Ndg^{ARod-G3.1}* embryos (B, C). (A-B) Stage 16 control (A) and *Ndg^{ARod-G3.1}* (B) mutant embryos stained with an anti-Ndg antibody (Ndg-B) that recognizes the region between the second G2 domain up to the fourth EGF repeat of Ndg [34]. (B) While *Ndg^{ARod-G3.1}* embryos do not show any Ndg staining in embryonic BMs, expression in chordotonal organs is unchanged (arrowheads). (C) *Ndg^{ARod-G3.1}* and *Ndg²* mutant embryos stained with an anti-Ndg antibody that recognizes an epitope in the Rod domain (Ndg-A; this work) do not show any staining. Scale bars represent 20µm (A-D). (TIF)

S4 Fig. Elimination of Ndg affects egg deposition, adult flight muscle BM and chill coma recovery. (A) Quantification of eggs laid by wild type (*w¹¹¹⁸*), *Ndg¹* and *Ndg²* virgin females. The curves join mean values of three experiments (individual dots). Differences with the wild type are significant in Kolmogorov-Smirnov tests (**: $p < 0.01$). (B) Images of eggs laid by wild type (*w¹¹¹⁸*), *Ndg¹* and *Ndg²* flies and graph quantifying egg aspect ratio (length/width). Each dot in the graph is a measurement from a single egg. Differences with the wild type were not significant in unpaired two-tailed Student's t tests. (C) Images of the BM (Vkg.GFP in green) of adult flight muscles, showing the BM is broken in *Ndg¹* mutants. (D) Quantification of chill

coma recovery time in adult female control flies, *Ndg*¹ mutant, *Ndg*² mutant, *Ndg*¹/*Df*(2*R*)*BSC281* and *Ndg*²/*Df*(2*R*)*BSC281*. Each dot in the graph is a measurement from a single fly. Differences with the wild type were significant in two-tailed t tests with Welch's correction (***: $p < 0.0001$). (B, D) Horizontal lines represent mean values.
(TIF)

S5 Fig. Nidogen constructs are secreted to the hemolymph. (A) Confocal images showing accumulation of secretion marker *secr.GFP* (signal peptide of Wg coupled to GFP, green) in pericardial filter cells of *Cg>secr.GFP* larvae. (B) Pericardial filter cells do not accumulate cytoplasmic GFP expressed in fat body and blood cells (*Cg>GFP.S65T*). (C) Confocal images of pericardial filter cells showing accumulation of GFP-tagged Ndg variants used in this study (see Fig 5). These variants were expressed in fat body and blood cells under control of *Cg-GAL4* and their presence in pericardial cells proves they are secreted. Nuclei stained with DAPI (blue).
(TIF)

S6 Fig. The Rod domain is essential for Ndg localization to BMs. Confocal images of the fat body, trachea, salivary gland, VNC, muscles and filter cells (secretion control) from *Cg>Ndg^{FL}.GFP* (upper panels) and *Cg>Ndg^{ΔRod}.GFP* (lower panels) larvae. GFP in green. Nuclei stained with DAPI (white).
(TIF)

S7 Fig. Regulation of Ndg.sGFP incorporation into BMs by Laminins, Col IV and Perlecan. Confocal images of the fat body BM showing localization of Ndg (Ndg.sGFP, green), laminin (*LanB1.sGFP*, cyan), Collagen IV (*Vkg.GFP*, green) and Perlecan (*Trol.YFP*). Images show fat body from wild type larvae (upper panels) and larvae where *LanA*, *LanB2* or *Cg25C* have been knocked down under control of *Cg-GAL4*.
(TIFF)

S1 Table. Numerical data and statistical analysis underlying all graphs in the manuscript.
(XLSX)

S2 Table. Full experimental genotypes.
(XLSX)

Acknowledgments

We thank Luis Garcia-Alonso, Jian-Quan Ni, Anne Holz, Bloomington Stock Center (Indiana, USA), National Institute of Genetics (Kyoto, Japan), *Drosophila* Genomics Resource Center (Kyoto, Japan), Vienna *Drosophila* Resource Center (Austria), Tsinghua Fly Center (Beijing, China) and *Drosophila* Carnegie Vector Collection (USA), Developmental Studies Hybridoma Bank (Iowa, USA) for sharing fly stocks, plasmids and antibodies. We also thank Georg Halder for co-supervision of Sofie Jacob's work.

Author Contributions

Conceptualization: Jianli Dai, Besaiz J. Sánchez-Sánchez, José C. Pastor-Pareja, María D. Martín-Bermudo.

Data curation: José C. Pastor-Pareja, María D. Martín-Bermudo.

Formal analysis: Jianli Dai, Beatriz Estrada, Sofie Jacobs, Besaiz J. Sánchez-Sánchez, Jia Tang, Mengqi Ma, Patricia Magadán-Corpas, José C. Pastor-Pareja, María D. Martín-Bermudo.

Funding acquisition: José C. Pastor-Pareja, María D. Martín-Bermudo.

Investigation: Jianli Dai, Beatriz Estrada, Sofie Jacobs, Besaiz J. Sánchez-Sánchez, Jia Tang, Mengqi Ma, Patricia Magadán-Corpas, José C. Pastor-Pareja, María D. Martín-Bermudo.

Methodology: Jianli Dai, Beatriz Estrada, Sofie Jacobs, Besaiz J. Sánchez-Sánchez, Jia Tang, Mengqi Ma, Patricia Magadán-Corpas, José C. Pastor-Pareja, María D. Martín-Bermudo.

Project administration: José C. Pastor-Pareja, María D. Martín-Bermudo.

Resources: José C. Pastor-Pareja, María D. Martín-Bermudo.

Software: José C. Pastor-Pareja, María D. Martín-Bermudo.

Supervision: José C. Pastor-Pareja, María D. Martín-Bermudo.

Validation: José C. Pastor-Pareja, María D. Martín-Bermudo.

Visualization: José C. Pastor-Pareja, María D. Martín-Bermudo.

Writing – original draft: Jianli Dai, José C. Pastor-Pareja, María D. Martín-Bermudo.

Writing – review & editing: Jianli Dai, Beatriz Estrada, José C. Pastor-Pareja, María D. Martín-Bermudo.

References

1. Yurchenco PD, Amenta PS, Patton BL. Basement membrane assembly, stability and activities observed through a developmental lens. *Matrix Biol.* 2004; 22(7):521–38. <https://doi.org/10.1016/j.matbio.2003.10.006> PMID: 14996432.
2. Carlin B, Jaffe R, Bender B, Chung AE. Entactin, a novel basal lamina-associated sulfated glycoprotein. *J Biol Chem.* 1981; 256(10):5209–14. PMID: 6262321.
3. Timpl R, Dziadek M, Fujiwara S, Nowack H, Wick G. Nidogen: a new, self-aggregating basement membrane protein. *Eur J Biochem.* 1983; 137(3):455–65. PMID: 6420150.
4. Fox JW, Mayer U, Nischt R, Aumailley M, Reinhardt D, Wiedemann H, et al. Recombinant nidogen consists of three globular domains and mediates binding of laminin to collagen type IV. *EMBO J.* 1991; 10(11):3137–46. PMID: 1717261; PubMed Central PMCID: PMC453035.
5. Reinhardt D, Mann K, Nischt R, Fox JW, Chu ML, Krieg T, et al. Mapping of nidogen binding sites for collagen type IV, heparan sulfate proteoglycan, and zinc. *J Biol Chem.* 1993; 268(15):10881–7. PMID: 8496153.
6. Ries A, Gohring W, Fox JW, Timpl R, Sasaki T. Recombinant domains of mouse nidogen-1 and their binding to basement membrane proteins and monoclonal antibodies. *Eur J Biochem.* 2001; 268(19):5119–28. PMID: 11589703.
7. Mann K, Deutzmann R, Timpl R. Characterization of proteolytic fragments of the laminin-nidogen complex and their activity in ligand-binding assays. *Eur J Biochem.* 1988; 178(1):71–80. PMID: 2462498.
8. Murshed M, Smyth N, Miosge N, Karolat J, Krieg T, Paulsson M, et al. The absence of nidogen 1 does not affect murine basement membrane formation. *Mol Cell Biol.* 2000; 20(18):7007–12. PMID: 10958695; PubMed Central PMCID: PMC453035.
9. Schymeinsky J, Nedbal S, Miosge N, Poschl E, Rao C, Beier DR, et al. Gene structure and functional analysis of the mouse nidogen-2 gene: nidogen-2 is not essential for basement membrane formation in mice. *Mol Cell Biol.* 2002; 22(19):6820–30. <https://doi.org/10.1128/MCB.22.19.6820-6830.2002> PMID: 12215539; PubMed Central PMCID: PMC453035.
10. Dong L, Chen Y, Lewis M, Hsieh JC, Reing J, Chaillet JR, et al. Neurologic defects and selective disruption of basement membranes in mice lacking entactin-1/nidogen-1. *Lab Invest.* 2002; 82(12):1617–30. PMID: 12480912.
11. Bader BL, Smyth N, Nedbal S, Miosge N, Baranowsky A, Mokkapaty S, et al. Compound genetic ablation of nidogen 1 and 2 causes basement membrane defects and perinatal lethality in mice. *Mol Cell Biol.* 2005; 25(15):6846–56. <https://doi.org/10.1128/MCB.25.15.6846-6856.2005> PMID: 16024816; PubMed Central PMCID: PMC453035.
12. Bose K, Nischt R, Page A, Bader BL, Paulsson M, Smyth N. Loss of nidogen-1 and -2 results in syndactyly and changes in limb development. *J Biol Chem.* 2006; 281(51):39620–9. <https://doi.org/10.1074/jbc.M607886200> PMID: 17023412.

13. Ackley BD, Kang SH, Crew JR, Suh C, Jin Y, Kramer JM. The basement membrane components nidogen and type XVIII collagen regulate organization of neuromuscular junctions in *Caenorhabditis elegans*. *J Neurosci*. 2003; 23(9):3577–87. PMID: [12736328](#).
14. Kang SH, Kramer JM. Nidogen is nonessential and not required for normal type IV collagen localization in *Caenorhabditis elegans*. *Mol Biol Cell*. 2000; 11(11):3911–23. <https://doi.org/10.1091/mbc.11.11.3911> PMID: [11071916](#); PubMed Central PMCID: [PMCPMC15046](#).
15. Kim S, Wadsworth WG. Positioning of longitudinal nerves in *C. elegans* by nidogen. *Science*. 2000; 288(5463):150–4. PMID: [10753123](#).
16. Durkin ME, Chakravarti S, Bartos BB, Liu SH, Friedman RL, Chung AE. Amino acid sequence and domain structure of entactin. Homology with epidermal growth factor precursor and low density lipoprotein receptor. *J Cell Biol*. 1988; 107(6 Pt 2):2749–56. PMID: [3264556](#); PubMed Central PMCID: [PMCPMC2115676](#).
17. Mayer U, Zimmermann K, Mann K, Reinhardt D, Timpl R, Nischt R. Binding properties and protease stability of recombinant human nidogen. *Eur J Biochem*. 1995; 227(3):681–6. PMID: [7867626](#).
18. Paulsson M, Aumailley M, Deutzmann R, Timpl R, Beck K, Engel J. Laminin-nidogen complex. Extraction with chelating agents and structural characterization. *Eur J Biochem*. 1987; 166(1):11–9. PMID: [3109910](#).
19. Poschl E, Mayer U, Stetefeld J, Baumgartner R, Holak TA, Huber R, et al. Site-directed mutagenesis and structural interpretation of the nidogen binding site of the laminin gamma1 chain. *EMBO J*. 1996; 15(19):5154–9. PMID: [8895559](#); PubMed Central PMCID: [PMCPMC452258](#).
20. Takagi J, Yang Y, Liu JH, Wang JH, Springer TA. Complex between nidogen and laminin fragments reveals a paradigmatic beta-propeller interface. *Nature*. 2003; 424(6951):969–74. <https://doi.org/10.1038/nature01873> PMID: [12931195](#)
21. Behrens DT, Villone D, Koch M, Brunner G, Sorokin L, Robenek H, et al. The epidermal basement membrane is a composite of separate laminin- or collagen IV-containing networks connected by aggregated perlecan, but not by nidogens. *J Biol Chem*. 2012; 287(22):18700–9. <https://doi.org/10.1074/jbc.M111.336073> PMID: [22493504](#); PubMed Central PMCID: [PMCPMC3365761](#).
22. Isabella AJ, Horne-Badovinac S. Building from the Ground up: Basement Membranes in *Drosophila* Development. *Curr Top Membr*. 2015; 76:305–36. <https://doi.org/10.1016/bs.ctm.2015.07.001> PMID: [26610918](#); PubMed Central PMCID: [PMCPMC4772872](#).
23. Natzle JE, Monson JM, McCarthy BJ. Cytogenetic location and expression of collagen-like genes in *Drosophila*. *Nature*. 1982; 296:368–71. PMID: [7063036](#)
24. Le Parco Y, Cecchini JP, Knibiehler B, Mirre C. Characterization and expression of collagen-like genes in *Drosophila melanogaster*. *Biol Cell*. 1986; 56(3):217–26. PMID: [3017484](#).
25. Yasothornsrikul S, Davis WJ, Cramer G, D.A. K, Dearolf CR. viking: identification and characterization of a second type IV collagen in *Drosophila*. *Gene*. 1997; 198:17–25. PMID: [9370260](#)
26. Kalluri R. Basement membranes: structure, assembly and role in tumour angiogenesis. *Nat Rev Cancer*. 2003; 3(6):422–33. <https://doi.org/10.1038/nrc1094> PMID: [12778132](#).
27. Borchiellini C, Coulon J, Le Parco Y. The function of type IV collagen during *Drosophila* embryogenesis. *Roux Arch Dev Biol*. 1996; 205(7–8):468–75. <https://doi.org/10.1007/BF00377228> PMID: [28306099](#).
28. Kiss M, Kiss AA, Radics M, Popovics N, Hermes E, Csiszar K, et al. *Drosophila* type IV collagen mutation associates with immune system activation and intestinal dysfunction. *Matrix Biol*. 2016; 49:120–31. <https://doi.org/10.1016/j.matbio.2015.09.002> PMID: [26363084](#).
29. Pastor-Pareja JC, Xu T. Shaping cells and organs in *Drosophila* by opposing roles of fat body-secreted Collagen IV and perlecan. *Dev Cell*. 2011; 21(2):245–56. <https://doi.org/10.1016/j.devcel.2011.06.026> PMID: [21839919](#); PubMed Central PMCID: [PMCPMC4153364](#).
30. Matsubayashi Y, Louani A, Dragu A, Sanchez-Sanchez BJ, Serna-Morales E, Yolland L, et al. A Moving Source of Matrix Components Is Essential for De Novo Basement Membrane Formation. *Curr Biol*. 2017; 27(22):3526–34 e4. <https://doi.org/10.1016/j.cub.2017.10.001> PMID: [29129537](#); PubMed Central PMCID: [PMCPMC5714436](#).
31. Timpl R, Rohde H, Robey PG, Rennard SI, Foidart JM, Martin GR. Laminin-a glycoprotein from basement membranes. *J Biol Chem*. 1979; 254:9933–37. PMID: [114518](#)
32. Yurchenco PD, Cheng YS. Self-assembly and calcium-binding sites in laminin. A three-arm interaction model. *J Biol Chem*. 1993; 268(23):17286–99. PMID: [8349613](#).
33. Urbano JM, Torgler CN, Molnar C, Tepass U, Lopez-Varea A, Brown NH, et al. *Drosophila* laminins act as key regulators of basement membrane assembly and morphogenesis. *Development*. 2009; 136(24):4165–76. Epub 2009/11/13. doi: dev.044263 [pii] <https://doi.org/10.1242/dev.044263> PMID: [19906841](#).

34. Wolfstetter G, Shirinian M, Stute C, Grabbe C, Hummel T, Baumgartner S, et al. Fusion of circular and longitudinal muscles in *Drosophila* is independent of the endoderm but further visceral muscle differentiation requires a close contact between mesoderm and endoderm. *Mech Dev*. 2009; 126(8–9):721–36. <https://doi.org/10.1016/j.mod.2009.05.001> PMID: 19463947.
35. Whitelock JM, Melrose J, Iozzo RV. Diverse cell signaling events modulated by perlecan. *Biochemistry*. 2008; 47(43):11174–83. <https://doi.org/10.1021/bi8013938> PMID: 18826258; PubMed Central PMCID: PMC2605657.
36. Datta S. Control of proliferation activation in quiescent neuroblasts of the *Drosophila* central nervous system. *Development*. 1995; 121(4):1173–82. PMID: 7743929.
37. Lindner JR, Hillman PR, Barrett AL, Jackson MC, Perry TL, Park Y, et al. The *Drosophila* Perlecan gene *trol* regulates multiple signaling pathways in different developmental contexts. *BMC Dev Biol*. 2007; 7:121. <https://doi.org/10.1186/1471-213X-7-121> PMID: 17980035; PubMed Central PMCID: PMC2174950.
38. Grigorian M, Liu T, Banerjee U, Hartenstein V. The proteoglycan *Trol* controls the architecture of the extracellular matrix and balances proliferation and differentiation of blood progenitors in the *Drosophila* lymph gland. *Dev Biol*. 2013; 384(2):301–12. <https://doi.org/10.1016/j.ydbio.2013.03.007> PMID: 23510717; PubMed Central PMCID: PMC24278754.
39. Philippakis AA, Busser BW, Gisselbrecht SS, He FS, Estrada B, Michelson AM, et al. Expression-guided in silico evaluation of candidate cis regulatory codes for *Drosophila* muscle founder cells. *PLoS Comput Biol*. 2006; 2(5):e53. <https://doi.org/10.1371/journal.pcbi.0020053> PMID: 16733548; PubMed Central PMCID: PMC21464814.
40. Urbano JM, Dominguez-Gimenez P, Estrada B, Martin-Bermudo MD. PS integrins and laminins: key regulators of cell migration during *Drosophila* embryogenesis. *PLoS One*. 2011; 6(9):e23893. <https://doi.org/10.1371/journal.pone.0023893> PMID: 21949686; PubMed Central PMCID: PMC3174947.
41. Zhu X, Ahmad SM, Aboukhalil A, Busser BW, Kim Y, Tansey TR, et al. Differential regulation of mesodermal gene expression by *Drosophila* cell type-specific Forkhead transcription factors. *Development*. 2012; 139(8):1457–66. <https://doi.org/10.1242/dev.069005> PMID: 22378636; PubMed Central PMCID: PMC3308180.
42. Hacker U, Kaufmann E, Hartmann C, Jurgens G, Knochel W, Jackle H. The *Drosophila* fork head domain protein *crocodile* is required for the establishment of head structures. *EMBO J*. 1995; 14(21):5306–17. Epub 1995/11/01. PMID: 7489720.
43. Sarov M, Barz C, Jambor H, Hein MY, Schmied C, Suchold D, et al. A genome-wide resource for the analysis of protein localisation in *Drosophila*. *Elife*. 2016; 5:e12068. <https://doi.org/10.7554/eLife.12068> PMID: 26896675; PubMed Central PMCID: PMC4805545.
44. Dai J, Ma M, Feng Z, Pastor-Pareja JC. Inter-adipocyte Adhesion and Signaling by Collagen IV Intercellular Concentrations in *Drosophila*. *Curr Biol*. 2017; 27(18):2729–40 e4. <https://doi.org/10.1016/j.cub.2017.08.002> PMID: 28867208.
45. Zang Y, Wan M, Liu M, Ke H, Ma S, Liu LP, et al. Plasma membrane overgrowth causes fibrotic collagen accumulation and immune activation in *Drosophila* adipocytes. *Elife*. 2015; 4:e07187. <https://doi.org/10.7554/eLife.07187> PMID: 26090908; PubMed Central PMCID: PMC4490375.
46. Ranganayakulu G, Elliott DA, Harvey RP, Olson EN. Divergent roles for NK-2 class homeobox genes in cardiogenesis in flies and mice. *Development*. 1998; 125(16):3037–48. PMID: 9671578.
47. Montell DJ, Goodman CS. *Drosophila* laminin: sequence of B2 subunit and expression of all three subunits during embryogenesis. *J Cell Biol*. 1989; 109(5):2441–53. Epub 1989/11/01. PMID: 2808533.
48. Petley-Ragan LM, Ardiel EL, Rankin CH, Auld VJ. Accumulation of Laminin Monomers in *Drosophila* Glia Leads to Glial Endoplasmic Reticulum Stress and Disrupted Larval Locomotion. *J Neurosci*. 2016; 36(4):1151–64. <https://doi.org/10.1523/JNEUROSCI.1797-15.2016> PMID: 26818504.
49. Haigo SL, Bilder D. Global tissue revolutions in a morphogenetic movement controlling elongation. *Science*. 2011; 331(6020):1071–4. Epub 2011/01/08. doi: [science.1199424](https://doi.org/10.1126/science.1199424) [pii] <https://doi.org/10.1126/science.1199424> PMID: 21212324.
50. Brac T. Charged sieving by the basal lamina and the distribution of anionic sites on the external surfaces of fat body cells. *Tissue Cell*. 1983; 15(3):489–98. PMID: 6612714.
51. Gibert P, Moreteau B, Petavy G, Karan D, David JR. Chill-coma tolerance, a major climatic adaptation among *Drosophila* species. *Evolution*. 2001; 55(5):1063–8. PMID: 11430643.
52. Zhang F, Zhao Y, Han Z. An in vivo functional analysis system for renal gene discovery in *Drosophila* pericardial nephrocytes. *J Am Soc Nephrol*. 2013; 24(2):191–7. <https://doi.org/10.1681/ASN.2012080769> PMID: 23291470; PubMed Central PMCID: PMC3559487.
53. Liu M, Feng Z, Ke H, Liu Y, Sun T, Dai J, et al. *Tango1* spatially organizes ER exit sites to control ER export. *J Cell Biol*. 2017; 216(4):1035–49. <https://doi.org/10.1083/jcb.201611088> PMID: 28280122; PubMed Central PMCID: PMC5379956.

54. Kim MJ, Choe KM. Basement membrane and cell integrity of self-tissues in maintaining *Drosophila* immunological tolerance. *PLoS Genet.* 2014; 10(10):e1004683. <https://doi.org/10.1371/journal.pgen.1004683> PMID: 25329560; PubMed Central PMCID: PMC4199487.
55. Henchcliffe C, Garcia-Alonso L, Tang J, Goodman CS. Genetic analysis of laminin A reveals diverse functions during morphogenesis in *Drosophila*. *Development.* 1993; 118(2):325–37. PMID: 8223265.
56. Brand AH, Perrimon N. Targeted gene expression as a means of altering cell fates and generating dominant phenotypes. *Development.* 1993; 118:401–15. PMID: 8223268
57. Phelps CB, Brand AH. Ectopic gene expression in *Drosophila* using GAL4 system. *Methods.* 1998; 14(4):367–79. <https://doi.org/10.1006/meth.1998.0592> PMID: 9608508.
58. Schwarzbauer J. Basement membranes: Putting up the barriers. *Curr Biol.* 1999; 9(7):R242–4. PMID: 10209113.
59. Timpl R. Macromolecular organization of basement membranes. *Curr Opin Cell Biol.* 1996; 8:618–24. PMID: 8939648
60. Miner JH, Yurchenco PD. Laminin functions in tissue morphogenesis. *Annu Rev Cell Dev Biol.* 2004; 20:255–84. Epub 2004/10/12. <https://doi.org/10.1146/annurev.cellbio.20.010403.094555> PMID: 15473841.
61. Poschl E, Schlotzer-Schrehardt U, Brachvogel B, Saito K, Ninomiya Y, Mayer U. Collagen IV is essential for basement membrane stability but dispensable for initiation of its assembly during early development. *Development.* 2004; 131(7):1619–28. Epub 2004/03/05. <https://doi.org/10.1242/dev.01037> dev.01037 [pii]. PMID: 14998921.
62. Aumailley M, Battaglia C, Mayer U, Reinhardt D, Nischt R, Timpl R, et al. Nidogen mediates the formation of ternary complexes of basement membrane components. *Kidney Int.* 1993; 43(1):7–12. PMID: 8433572.
63. Ekblom P, Ekblom M, Fecker L, Klein G, Zhang HY, Kadoya Y, et al. Role of mesenchymal nidogen for epithelial morphogenesis in vitro. *Development.* 1994; 120(7):2003–14. PMID: 7925005.
64. Kadoya Y, Salmivirta K, Talts JF, Kadoya K, Mayer U, Timpl R, et al. Importance of nidogen binding to laminin gamma1 for branching epithelial morphogenesis of the submandibular gland. *Development.* 1997; 124(3):683–91. PMID: 9043083.
65. Yurchenco PD, Ruben GC. Basement membrane structure in situ: evidence for lateral associations in the type IV collagen network. *J Cell Biol.* 1987; 105(6 Pt 1):2559–68. PMID: 3693393; PubMed Central PMCID: PMC42114722.
66. LeBleu VS, Macdonald B, Kalluri R. Structure and function of basement membranes. *Exp Biol Med (Maywood).* 2007; 232(9):1121–9. <https://doi.org/10.3181/0703-MR-72> PMID: 17895520.
67. Hosler JS, Burns JE, Esch HE. Flight muscle resting potential and species-specific differences in chill-coma. *J Insect Physiol.* 2000; 46(5):621–7. PMID: 10742510.
68. Lossl P, Kolbel K, Tanzler D, Nannemann D, Ihling CH, Keller MV, et al. Analysis of nidogen-1/laminin gamma1 interaction by cross-linking, mass spectrometry, and computational modeling reveals multiple binding modes. *PLoS One.* 2014; 9(11):e112886. <https://doi.org/10.1371/journal.pone.0112886> PMID: 25387007; PubMed Central PMCID: PMC4227867.
69. Patel TR, Bernardis C, Meier M, McEleney K, Winzor DJ, Koch M, et al. Structural elucidation of full-length nidogen and the laminin-nidogen complex in solution. *Matrix Biol.* 2014; 33:60–7. <https://doi.org/10.1016/j.matbio.2013.07.009> PMID: 23948589.
70. Hopf M, Gohring W, Ries A, Timpl R, Hohenester E. Crystal structure and mutational analysis of a perlecan-binding fragment of nidogen-1. *Nat Struct Biol.* 2001; 8(7):634–40. <https://doi.org/10.1038/89683> PMID: 11427896.
71. Kvensakul M, Hopf M, Ries A, Timpl R, Hohenester E. Structural basis for the high-affinity interaction of nidogen-1 with immunoglobulin-like domain 3 of perlecan. *EMBO J.* 2001; 20(19):5342–6. <https://doi.org/10.1093/emboj/20.19.5342> PMID: 11574465; PubMed Central PMCID: PMC42125277.
72. Willem M, Miosge N, Halfter W, Smyth N, Jannetti I, Burghart E, et al. Specific ablation of the nidogen-binding site in the laminin gamma1 chain interferes with kidney and lung development. *Development.* 2002; 129(11):2711–22. PMID: 12015298.
73. Paulsson M. Basement membrane proteins: structure, assembly, and cellular interactions. *Crit Rev Biochem Mol Biol.* 1992; 27(1–2):93–127. <https://doi.org/10.3109/10409239209082560> PMID: 1309319.
74. Yurchenco PD, Tsilibary EC, Charonis AS, Furthmayr H. Models for the self-assembly of basement membrane. *J Histochem Cytochem.* 1986; 34(1):93–102. <https://doi.org/10.1177/34.1.3510247> PMID: 3510247.
75. Roote J, Prokop A. How to design a genetic mating scheme: a basic training package for *Drosophila* genetics. *G3 (Bethesda, Md).* 2013; 3(2):353–8. Epub 2013/02/08. <https://doi.org/10.1534/g3.112.004820> PMID: 23390611; PubMed Central PMCID: PMC4213564995.

76. Halfon MS, Gisselbrecht S, Lu J, Estrada B, Keshishian H, Michelson AM. New fluorescent protein reporters for use with the *Drosophila* Gal4 expression system and for vital detection of balancer chromosomes. *Genesis*. 2002; 34(1–2):135–8. <https://doi.org/10.1002/gene.10136> PMID: 12324968.
77. Witsell A, Kane DP, Rubin S, McVey M. Removal of the bloom syndrome DNA helicase extends the utility of imprecise transposon excision for making null mutations in *Drosophila*. *Genetics*. 2009; 183(3):1187–93. <https://doi.org/10.1534/genetics.109.108472> PMID: 19687136; PubMed Central PMCID: PMC2778970.
78. Martinek N, Shahab J, Saathoff M, Ringuette M. Haemocyte-derived SPARC is required for collagen-IV-dependent stability of basal laminae in *Drosophila* embryos. *J Cell Science*. 2008; 121:1671–8. <https://doi.org/10.1242/jcs.021931> PMID: 18445681
79. Voigt A, Pflanz R, Schafer U, Jackle H. Perlecan participates in proliferation activation of quiescent *Drosophila* neuroblasts. *Dev Dyn*. 2002; 224(4):403–12. Epub 2002/08/31. <https://doi.org/10.1002/dvdy.10120> PMID: 12203732.
80. Vert JP, Foveau N, Lajaunie C, Vandenbrouck Y. An accurate and interpretable model for siRNA efficacy prediction. *BMC bioinformatics*. 2006; 7:520. Epub 2006/12/02. <https://doi.org/10.1186/1471-2105-7-520> PMID: 17137497; PubMed Central PMCID: PMC1698581.
81. Ni JQ, Zhou R, Czech B, Liu LP, Holderbaum L, Yang-Zhou D, et al. A genome-scale shRNA resource for transgenic RNAi in *Drosophila*. *Nature methods*. 2011; 8(5):405–7. Epub 2011/04/05. <https://doi.org/10.1038/nmeth.1592> PMID: 21460824; PubMed Central PMCID: PMC3489273.
82. Spradling AC. P element-mediated. In Roberts D.B. (ed.), *Drosophila: A Practical Approach*. IRL Press, Oxford, pp. 175–197. 1986.
83. Ren X, Sun J, Housden BE, Hu Y, Roesel C, Lin S, et al. Optimized gene editing technology for *Drosophila melanogaster* using germ line-specific Cas9. *Proceedings of the National Academy of Sciences of the United States of America*. 2013; 110(47):19012–7. Epub 2013/11/06. <https://doi.org/10.1073/pnas.1318481110> PMID: 24191015; PubMed Central PMCID: PMC3839733.
84. Port F, Chen HM, Lee T, Bullock SL. Optimized CRISPR/Cas tools for efficient germline and somatic genome engineering in *Drosophila*. *Proc Natl Acad Sci U S A*. 2014; 111(29):E2967–76. <https://doi.org/10.1073/pnas.1405500111> PMID: 25002478; PubMed Central PMCID: PMC4115528.
85. Frydman HM, Spradling AC. The receptor-like tyrosine phosphatase *lar* is required for epithelial planar polarity and for axis determination within *drosophila* ovarian follicles. *Development*. 2001; 128(16):3209–20. Epub 2001/11/02. PMID: 11688569.